Control of replication associated DNA damage responses by Mismatch Repair

Ijsselsteiijn, R.

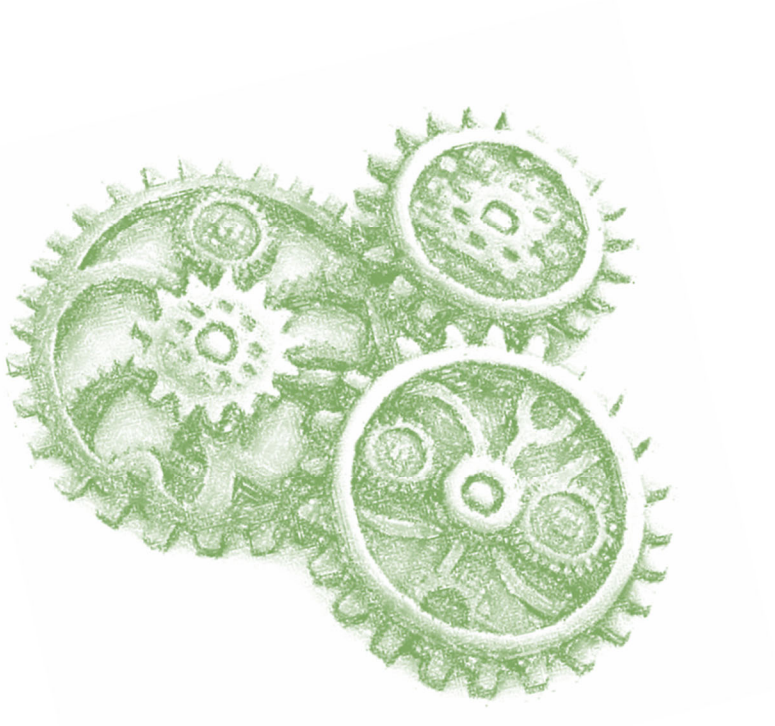

Chapter 3:

Characterizing the role of mismatch repair components in the ultraviolet light-induced post-translesion synthesis repair pathway

Robbert Ijsselsteijn[1], Gido Snaterse[1], Mark Drost[1], Jacob G Jansen[1]

[1]Department of Human Genetics, Leiden University Medical Center, Leiden, The Netherlands.

Abstract

DNA mismatch repair (MMR) removes base-base misincorporations that are generated by the replicative DNA polymerases delta and epsilon to prevent mutagenesis. Previous work has suggested that the apical MMR heterodimer MutSα (Msh2/Msh6) also suppresses UV-induced mutagenesis and concomitantly activates DNA damage signaling, possibly by generating ssDNA tracts covered with Replication Protein A (RPA). To identify additional MMR-related genes that may play a role in these non-canonical activities of MutSα we here analyzed responses to UV light of nucleotide excision repair (NER)-deficient mouse embryonic stem (mES) cells with an additional defect in MMR-components Mlh1 or Pms2 that form the heterodimer MutLα, in Mlh1-interacting proteins Mlh3 or Pms1, and in exonucleases Exo1 or Fan1. These experiments show that MutLα suppresses UV-induced mutagenesis to a similar extent as MutSα, however, in contrast to MutSα, MutLα is not required for activating UV-induced DNA damage signaling. Mutation spectra analyses of the Hprt gene are compatible with a model where MutSα and MutLα suppress UV-induced mutagenesis by removing misincorporations opposite photolesions at pyrimidine dimers. In contrast, Pms1, Mlh3, Fan1 and Exo1 do not play a role in the suppression of UV-induced mutagenesis or in DNA damage signaling. In conclusion, our data reveal that MutLα suppresses UV-induced mutagenesis independent of activating UV-induced damage signaling, indicating a separation of function between MutSα and its downstream actor MutLα in response to UV-induced DNA damage.

Introduction

DNA mismatch repair (MMR) is an evolutionarily conserved genome maintenance pathway best known for correcting mis-incorporations introduced by replicative DNA polymerases opposite unmodified nucleotides in DNA. The canonical MMR pathway consists of mismatch recognition, nick-dependent excision and gap filling. More specifically, eukaryotic MMR initiates with either the heterodimeric protein complex MSH2/MSH6 (MutSα) that recognizes base/base mispairs and 1-2 base pair insertion/deletion loops or with the MSH2/MSH3 (MutSβ) complex that recognizes larger insertion/deletion loops. Then, recruitment of the heterodimer MLH1/PMS2 (MutLα), displaying endonucleolytic activity, is critical for the excision of the newly synthesized strand containing the mismatched nucleotide. This endonuclease can generate an incision 5' to the mismatch in the newly synthesized strand. MutLα is also important in 3' nick-directed MMR (1). Subsequently, the mis-incorporation can be removed by multiple pathways that either depend on long-range exonucleolytic resection by EXO1, continued endonucleolytic degradation by MutLα or strand displacement by replicative DNA polymerase delta followed by 5' flap cleavage (2). Any remaining single stranded DNA (ssDNA) is converted into double stranded DNA (dsDNA) by DNA polymerase delta and the remaining nick is sealed by a DNA ligase (1). Other exonucleases beside EXO1 may act redundantly in removal of misincorporations, like FANCI-associated nuclease 1 (FAN1), that is shown to interact with MSH2 and MLH1 after treatment with the MMR-inducing methylating agent N-methyl-N-nitrosourea (MNU) (3). MLH1 also interacts with MMR homologs PMS1 and MLH3 thereby forming MutLβ and MutLγ, respectively. The amino acid sequence of *MLH3* is most similar to the sequence of *PMS2*, suggesting that they may display overlapping functions. Mammalian MutLγ exhibits endonuclease activity at loop-containing DNA (4) and deficiency of mouse Mlh3 leads to a low, but significant, increase of mutations at microsatellites, a phenotype indicative of defective MMR. Moreover, loss of both Pms2 and Mlh3 results in microsatellite instability comparable to loss of their binding partner Mlh1, suggesting functional redundancy between Pms2 and Mlh3 (5). The role of PMS1 is much more enigmatic and to date no clear phenotypes of PMS1 loss have been found (6).

Apart from operating in canonical MMR, several MMR proteins seem to play an important role in the response to damaged nucleotides such as bulky and helix-distorting photolesions induced by ultraviolet (UV) light. As they form strong blocks for replicative DNA polymerases, these lesions are bypassed by specialized translesion synthesis (TLS) polymerases to allow completion of DNA replication. However, due to low replication fidelity and lack of proofreading, TLS polymerases frequently misincorporate opposite UV lesions (7). Basepairing between these helix-distorting DNA lesions and 'mismatched' nucleotides is severely perturbed or absent. Nonetheless, purified MutSα is able to preferentially bind these compound structures *in vitro* (8). In addition, MSH2 and MSH6 are important for inducing an UV-induced cell cycle arrest and apoptotic responses in human melanoma cells (9), in mouse epidermal cells *in vivo*, in mouse keratinocytes and in mouse embryonic stem (mES)

cells (10, 11). Furthermore, although MutSα does not seem to play a role in the removal of photolesions, rodent cells defective for Msh2, Msh6 or Pms2 display increased UV-induced mutagenesis compared to MMR proficient cells (12-14). Mice defective for Msh2 show accelerated skin tumorigenesis following UVB exposure (15, 16), underscoring the protective role of Msh2 in genome stability in response to UV light.

In replicating cells the early responses following UV exposure are accompanied with MutSα-dependent formation of ssDNA tracts that encompass UV photolesions (11). These patches of ssDNA are coated with the ssDNA binding heterotrimeric protein Replication Protein A (RPA) that activates a signaling cascade via the sensor checkpoint kinase Ataxia Telangiectasia and Rad3-related protein (ATR), resulting in the activation of effector kinases such as Chk1 that are important for activating a cell cycle arrest (17). Based on the MutSα-dependent suppression of UV-induced mutagenesis and findings that most UV-induced mutations in MutSα-deficient cells are likely targeted at UV lesions, it has been proposed that these ssDNA patches result from MutSα-dependent removal of the 'mismatched' nucleotides opposite photolesions. Together these data led to the hypothesis of a non-canonical MMR pathway, dubbed post-TLS repair, that controls TLS-associated mutagenesis by removal of misincorporations opposite helix-distorting nucleotide lesions, whilst the excision tracts activate DNA damage signaling cascades, resulting in cell cycle arrest and apoptotic responses (11).

In the present study we asked whether MMR-related proteins other than MutSα contribute to the suppression of UV-induced mutations and the concomitant induction of cell cycle arrest and apoptotic responses. To this end isogenic mES cell lines were generated with single defects in the canonical MMR genes *Mlh1* and *Pms2*, in *Mlh3* and *Pms1* and in MMR-associated exonucleases *Exo1* and *Fan1*. These cell lines contain an additional defect in the *Xpa* gene, a core factor in nucleotide excision repair, to exclude removal of UV photolesions. We show that the generation of UV-induced ssDNA and the activation of DNA damage signaling depend on Msh6, but not on the downstream factors of canonical MMR, including MutLα. However, UV-induced mutagenesis is controlled not only by MutSα but also by Mlh1 and Pms2, indicating a role of MutLα in controlling the mutagenicity of helix-distorting DNA lesions. Mutation spectra analysis of mutations in the *Hprt* gene revealed that UV-induced mutations were dominated by C > T transitions at dipyrimidine sites, which were predominantly located in the transcribed strand, irrespective of Msh6 or Mlh1 status. Neither the Mlh1-interacting proteins Mlh3 and Pms1 nor the MMR-associated exonucleases Exo1 and Fan1 play an overt role in post-TLS repair. Taken together these data suggest an uncoupling of the DNA damage signaling induced by UV, which only depends on Msh6, from the control of UV-induced mutagenesis, which requires all of the core MMR proteins.

Materials and Methods

Cell lines and cell culture

Wild-type mES cells were used as a parental line to all cell lines acquired (18). The *Xpa* deficient cell line was previously generated by Hendriks et al. (2010) through targeted disruption of exons 3 and 4. Deficiencies for *Mlh3*, *Pms1*, *Exo1* and *Fan1* in the *Xpa* deficient cell line were introduced using CRISPR/Cas9 (Supplementary methods table 2). The *Mlh3* deficient cell lines are disrupted by a frameshifting deletion in exon 6, the *Pms1* deficient cell lines have frameshifting deletions in exon 10, the *Exo1* cell lines are disrupted in exon 5 or 6 and the *Fan1* cell lines have their entire genes deleted. The cell lines were validated using RT-PCR analysis (Fig. S1). The *Exo1* cell lines were still able to produce shortened mRNA, whereas all other cell lines did not produce stable mRNA from the disrupted gene. The MMR deficient cell lines for *Msh6*, *Mlh1* and *Pms2* were made deficient by using CRISPR/Cas9 constructs targeting exon 1-2 for *Msh6*, the entire gene for *Mlh1* and exons 5-7 for *Pms2*, respectively, and were afterwards selected for MMR deficiency following a (40μM) 6tG treatment for four hours. Knock-out was validated by western blot (Fig. S1). ES cells were cultured on senescent mouse embryonic fibroblast feeder cells in complete medium consisting of DMEM KO (Gibco) supplemented with 10% fetal calf serum (Bodinco/Capricorn Scientific), 1% glutamax (Gibco), 1% non-essential amino acids (Gibco), 1mM pyruvate (Gibco), 100U penicillin/100μg streptomycin (Gibco), 0.1mM β-mercapto-ethanol (Sigma-Aldrich) and leukemia inhibitory factor (LIF, made in house). During experiments complete medium was mixed in a 1:1 ratio with Buffalo rat liver (BRL) cell-conditioned medium called 50/50 to allow for growth on gelatin-coated culture dishes.

Determination of UV-induced DNA damage signaling

One million cells were seeded in gelatin-coated 6 wells plates with 50/50 medium one day prior to exposure with 0,75J/m^2 of UV-C. Following UV treatment cells were cultured in 50/50 medium. Cells were lysed using 300μl 2x Laemmli sample buffer 0, 2, 4 and 8 hours after UV-C exposure. In some experiments nocodazole (300 ng/ml) (Sigma Aldrich) was added immediately after UV irradiation to block cells in mitosis. Samples were loaded on SDS-PAGE using 12.5μl sample per slot of a 4-12% Criterion XT Bis-Tris Gel (Bio-rad). Proteins were transferred onto Protran 0.45μM nitrocellulose membranes (GE Healthcare) using 400mA (~70V) for 2 hours at 4°C. Then, nitrocellulose membranes were incubated with Rockland blocking reagent (Rockland) diluted 1:1 with 0.1% PBS-Tween (Rockland-PBS-T) for one hour to block non-specific antibody binding. Afterwards, membranes were incubated in Rockland-PBS-T with primary antibodies against Kap-1^p (1:1000, Bethyl, polyclonal A300-767A), Chk1^p (1:1000, Cell signaling technology, clone 133D3) or PCNA (1:8000, Santa Cruz, clone PC10) for overnight at 4°C. The next day the membranes were washed with PBS-tween (0.1%) and incubated with secondary anti-rabbit and anti-mouse HRP (1:50000 in Rockland-PBS-T) depending on the primary antibody isotype. Amersham ECL select (GE Healthcare) was used to visualize protein bands.

Subcellular fractionation and the analysis of chromatin-bound Rpa

1.5 million cells were seeded in gelatin-coated 60mm dishes in 50/50 medium and grown for a day. The cells were washed twice with PBS before exposure to 2J/m^2 of UV and incubated in 50/50 medium for 0 or 4 hours. Next, cells were collected by trypsinization and 2 million cells were used for fractionation using the Subcellular Protein Fractionation Kit for Cultured Cells (Thermo Fisher Scientific) according to the manufacturer's recommendation. The total amount of protein in the isolated fractions was measured using a Bradford assay (Thermo Fisher Scientific). SDS-PAGE was performed with 10µg of protein per sample using 4-12% Criterion XT Bis-Tris Gels (Bio-rad). Western blot was performed as described previously with antibodies against Histone H3 (Abcam, polyclonal) and Rpa (Cell signaling technology, Clone 4E4).

Determination of *Hprt* mutant frequency

Per condition, five million cells were seeded in 50/50 medium in a 90mm dish coated with gelatin and grown for one day. Then, cells were washed twice with PBS, exposed to 0 or 0.75J/m^2 UV, and 5 million cells were seeded into a new gelatin-coated dish with 50/50 medium. Cell populations were split every two days for three passages. Then, 2 million cells were equally distributed over 5 gelatin-coated 90mm dishes containing 50/50 medium with 30µM 6tG. In parallel 250 cells were seeded in gelatin-coated 60mm dishes in triplicate to determine the clone forming ability. The clones were grown 7-10 days before staining with methylene blue. The number of clones was determined by manual counting. The frequency of 6tG resistant clones per million cells was adjusted for the cloning efficiency.

Next generation sequencing of clones selected for *Hprt* inactivation

For mock treated XpaMsh6 and XpaMlh1 cells and for UV exposed Xpa, XpaMsh6 and XpaMlh1 cells approximately 400 6tG clones were collected by trypsinization and lysed in 1.6ml TRIzol reagent (Invitrogen). Total RNA was isolated following manufacturer's protocol and ultimately dissolved in 15µl TE buffer. To generate cDNA 1 µl RNA was mixed with dNTPs (0.2mM Invitrogen) and 5 µM primer 1 (Supplemental materials table 1) in a final volume of 14.5µl and incubated for 5 minutes at 65°C. Then, a mixture of 5.5µl consisting of 1µl Maxima H Minus Reverse Transcriptase (200U) (Thermo Fisher Scientific), 4µl 5x Maxima buffer and 0.5µl RNAsin (20U) (Promega) was added followed by incubations at 57°C for one hour and at 85°C for 5 minutes, respectively. 2µl of cDNA was used in a PCR with 0.4U Phusion High-Fidelity DNA polymerase (Thermo Fisher Scientific), 5x Phusion PCR buffer, dNTPs (0.2mM), and a combination of forward and reverse primers (0.5µM) (Supplemental materials table 1), depending on which amplicon of *Hprt* is amplified (primers 2/3, 4/5, 6/1). Using a thermal cycler, PCR products were generated by incubating the reaction mixture for two minutes at 95°C, followed by 15 seconds at 95°C, 30 seconds at 57°C and one minute 72°C for 25 cycles, and a final elongation step of 72°C for five minutes. AMPure XP beads (Beckman Coulter) were used to purify the PCR products in 20µl deionized H_2O following manufacturer's protocol. These PCR products were used as templates for Phusion PCR with barcoded primers (primers 7/8, 9/10, 11/12, 13/14, 15/16, 17/18) as

previously described, with the exception of 8 instead of 25 cycles. Barcoded PCR products were purified with AMPure beads and the size of the purified products was measured using a Qiaxcel Advanced System (Qiagen). Finally, 50ng pooled PCR products was sequenced using Illumina Paired-End sequencing (GenomeScan).

Determination of UV-induced mutational spectra in the *Hprt* coding region

Raw next generation sequencing data was first filtered to contain reads with a maximum error probability of 0.05. Using Flash (19) paired-end reads were merged and mapped to the *Hprt* reference sequence using in-house software (20). Additional filters removed reads that did not start or end with the primer combinations that were used to obtain the PCR fragments. Finally, the mapped reads were compared to the *Hprt* sequence and annotated into WT (wild-type), single nucleotide substitution (SNS), multi nucleotide substitution (MNS), deletion or insertion. Unique mutations were considered to be real if the allele frequency was > 0.001, anything below that threshold is considered noise.

Results

UV-induced DNA damage signaling depends on MutSα, but not on MutLα

Previously, it was shown that Msh6 is important for the activation of DNA damage signaling upon UV exposure, possibly via excision of TLS-induced misincorporations opposite UV lesions (11). Here, the importance of other MMR-related genes in the activation of UV-induced damage responses was studied using *Xpa*-deficient mES cells with an additional deficiency for (i) the canonical MMR proteins and MutLα constituents Mlh1 or Pms2, that act downstream of MutSα, (ii) the Mlh1-interacting proteins Mlh3 and Pms1 and (iii) MMR-associated exonucleases Exo1 and Fan1. UV-induced DNA damage signaling was studied by western blotting for phosphorylated forms of Chk1 and Kap-1, that are substrates for the Atr/Atrip and Atm kinases, respectively. *Xpa*-deficient cells displayed significant phosphorylation of Chk1 and Kap-1, 2 to 8 hours after UV exposure, which was greatly reduced when these cells lacked *Msh6* (Fig. 1), in line with previously published work (11). UV-exposed cells deficient for *Mlh1* or *Pms2*, however, showed similar levels of phosphorylated Chk1 as the MMR proficient controls, and phosphorylation of Kap-1 appeared slightly reduced although not as much as in *Msh6* cells (Fig. 1, S2). This indicates that Mlh1 and Pms2 play a less important role than Msh6 in activating UV-induced DNA damage signaling. Similar results were found for cell lines deficient for *Mlh3*, *Pms1*, *Exo1* and *Fan1*. Together these data indicate that only MutSα plays a significant role in activating UV-induced DNA damage signaling.

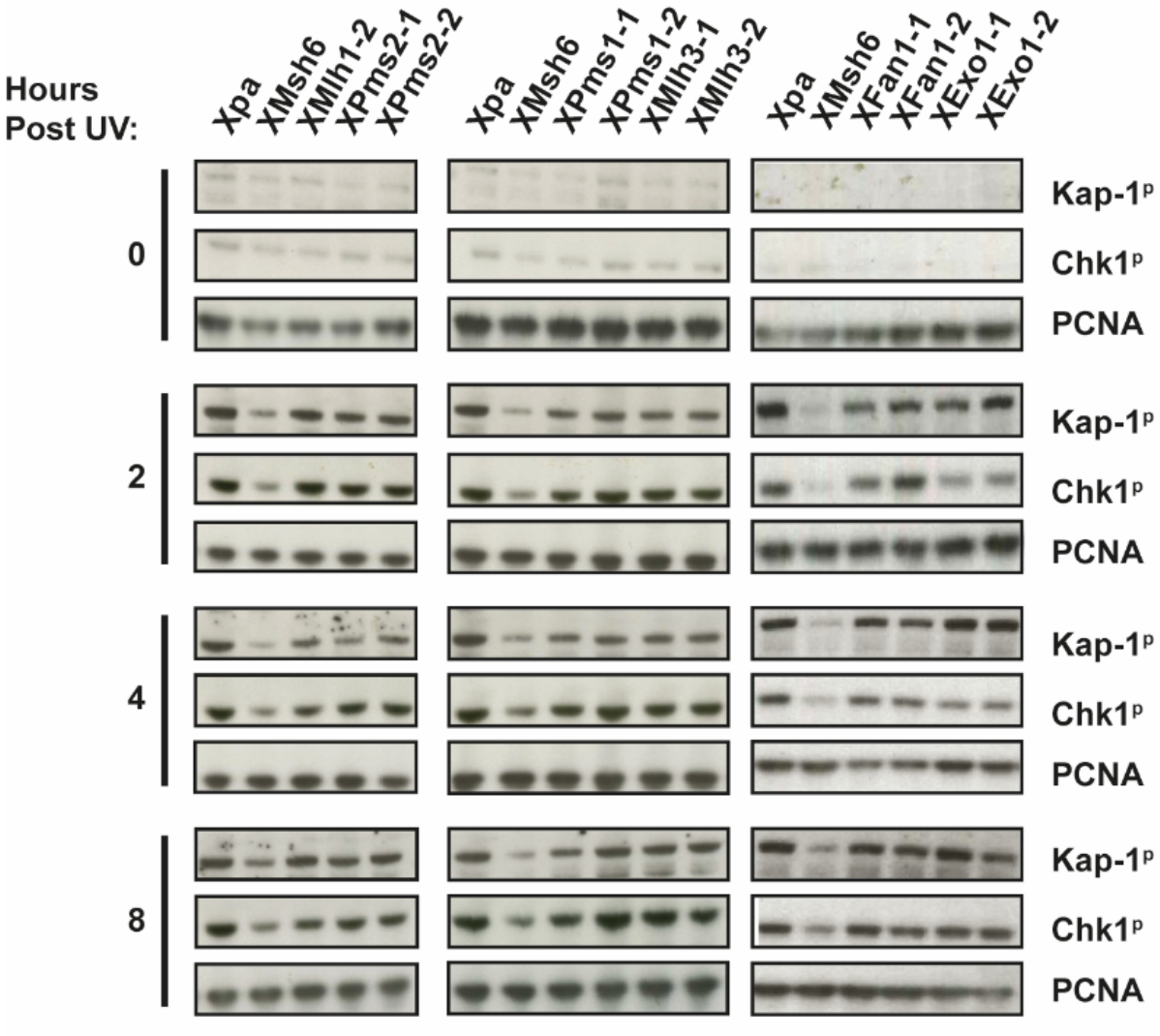

Figure 1: UVC-induced DNA damage signaling in cell lines deficient for MMR, MMR homologs and exonucleases

Western blots displaying formation of Chk1p and Kap-1p in Xpa, XMsh6, XMlh1, XPms2, XMlh3, XPms1, XExo1 and XFan1 deficient lines, 0, 2, 4 and 8 hours post UVC exposure (0,75J/M2). PCNA was used as a loading control. Cell line-1 -2, denotes independent cell lines with different inactivating mutations. Representative images of 3 independent experiments. X=Xpa deficiency.

Msh6 promotes UV-induced single stranded DNA formation and checkpoint activation independent of *Mlh1*

We asked whether the persistence of UV damage signaling in Mlh1-deficient cells relies on MutSα. To test this, we generated an *XpaMlh1Msh6* triple knockout cell line and compared the formation of pChk1 in *Xpa*, *XpaMsh6*, *XpaMlh1* and *XpaMlh1Msh6* cells following UV exposure. We found that UV-induced DNA damage signaling in Mlh1-deficient cells strongly depends on Msh6, since the level of pChk1 observed in UV-exposed *XpaMlh1* cells was completely absent in the *XpaMlh1Msh6* triple knock out cells (Fig. 2A). Of note, the activation of Chk1 in *Xpa* and *XpaMlh1* cells occurs during the cell cycle of UV exposure as shown by arresting UV-exposed cells at mitosis following nocodazole treatment (Fig. S3A).

MutSα may activate checkpoint signaling in different ways, *i.e.* by a direct interaction with Atr/Atrip following mismatch binding (21) or by generating patches of ssDNA, which relies on the recruitment of MutLα in case 5' nicking is required for excision (22). To distinguish between these modes of checkpoint activation, we analyzed the formation of ssDNA by western blotting for chromatin-bound RPA, a heterotrimeric protein that specifically binds to ssDNA. In the *Xpa*-deficient cell line an increase of chromatin-bound RPA was observed, 4 hours after UV irradiation. This increase completely depends on the presence of Msh6, since its loss resulted in absence of chromatin-bound RPA induced by UV (Fig. 2B-D, S3B). Conversely, *Xpa* cells deficient for Mlh1 or its binding partner Pms2 showed similar increased levels of chromatin-bound RPA as found for *Xpa* cells following UV exposure. These data suggest that the formation of UV-induced ssDNA is dependent on Msh6, but not on MutLα.

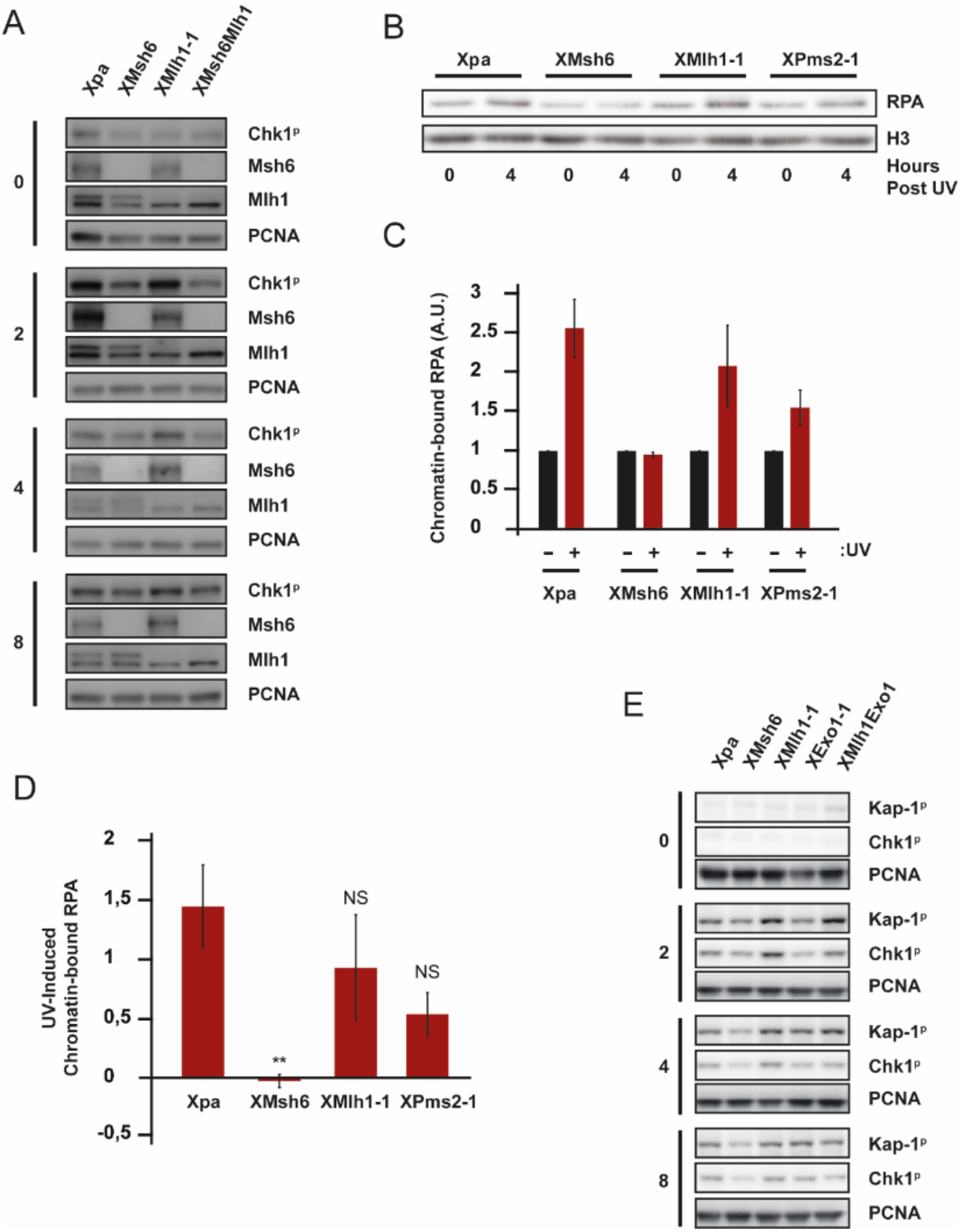
A
Xpa
XMsh6
XMlh1-1
XMsh6Mlh1
0
2
4
8
Chk1P
Msh6
Mlh1
PCNA
B
Xpa
XMsh6
XMlh1-1
XPms2-1
RPA
H3
0 4 0 4 0 4 0 4
Hours Post UV
C
Chromatin-bound RPA (A.U.)
3
2.5
2
1.5
1
0.5
0
- + - + - + - + :UV
Xpa
XMsh6
XMlh1-1
XPms2-1
D
UV-Induced Chromatin-bound RPA
2
1,5
1
0,5
0
-0,5
**
NS
NS
Xpa
XMsh6
XMlh1-1
XPms2-1
E
Xpa
XMsh6
XMlh1-1
XExo1-1
XMlh1Exo1
0
2
4
8
Kap-1P
Chk1P
PCNA

Figure 2: Msh6 dependent formation of chromatin-bound Rpa and DNA damage signaling following UVC exposure
A: Western blots showing formation of Chk1p in Xpa, XMsh6, XMlh1 and XMsh6Mlh1 cell lines, 0, 2, 4 and 8 hours post UVC exposure (0,75J/M2). Msh6 and Mlh1 protein status was confirmed using appropriate antibodies against Msh6 and Mlh1. PCNA was used as a loading control. Representative images of 3 independent experiments. B: Western blot of chromatin-bound Rpa as a measure for the formation of single stranded DNA, 0 and 4 hours post UVC exposure (2J/M2). Histone H3 (H3) was used as a loading control. Representative image of three independent experiments. C: Quantification of chromatin-bound Rpa. Samples were normalized to the 0-hours timepoint and adjusted for the amount of Histone H3. Error-bars, SEM. D: UVC-induced chromatin-bound Rpa. Error bars, SEM. **, P ≤ 0,01, ns, not statistically significant; unpaired T-test comparing groups to WT. E: Western blots displaying formation of Chk1p and Kap-1p in Xpa, XMsh6, XMlh1, XExoI and XMlh1ExoI cell lines, 0, 2, 4 and 8 hours post UVC exposure (0,75J/M2). Msh6 protein status was confirmed using Msh6 antibodies. Representative images of 3 independent experiments. X=Xpa deficiency.

Recently, it was shown that loss of Mlh1 leads to Exo1-dependent hyper-resection at DNA breaks induced by ionizing radiation, resulting in enhanced loading of RPA on DNA and, consequently, increased damage signaling (23). To test whether the UV-induced damage signaling in Mlh1-deficient cells relies on Exo1, we inactivated *Exo1* in *XpaMlh1* cells by Cas/Crispr, exposed the resulting *XpaMlh1Exo1* triple knock-out cells to UV light and determined phosphorylation levels of Chk1 and Kap-1. We found slightly increased levels of pChk1 and pKap-1 in *XpaMlh1Exo1* cells as compared to *Xpa* and *XpaMlh1* cells across most timepoints post-UV exposure (Fig. 2E), indicating that the DNA damage signaling found in *XpaMlh1*-deficient cells does not rely on *Exo1*. This result is in line with the wild type level of Chk1 phosphorylation in *XpaExo1* cells (Fig. 1 and 2E). Together these data indicate that, following UV exposure, the formation of ssDNA and concomitant activation of the RPA/Atr/Chk1 signaling cascade strongly depends on Msh6 and not on its downstream actor MutLα.

UV-induced mutagenesis is controlled by multiple MMR proteins

Msh6-dependent UV damage signaling is associated with protecting cells from UV-induced mutagenesis, possibly via the removal of TLS-induced mis-incorporations opposite UV lesions, resulting in the formation of ssDNA gaps (11). Since MutLα is not required for UV-induced checkpoint responses and formation of ssDNA, we wondered whether MutLα is dispensable for protecting against UV-induced mutagenesis as well. To address this, we determined mutant frequencies at the X-linked *Hprt* gene in mES cells deficient for the *Xpa* gene and in cells carrying an additional deficiency for *Mlh1* or *Pms2*. We also included cell lines with defects in Mlh1-interacting proteins Mlh3 or Pms1 and in exonucleases Exo1 or Fan1. *Hprt* mutants can be selected from Hprt-proficient cells by using 6tG as selective agent. Exposing *Xpa* cells to 0,75J/m^2 UV led to a minor increase of 34.02±17.76 x 10^{-6} 6tG-resistant clones compared to mock-treated *Xpa* cells (Fig. 3A, S4A, S4C). Loss of *Msh6* in an *Xpa*-deficient background resulted in 108.46±22.26 x 10^{-6} 6tG-resistant clones in unexposed cells, which further increased to 502.11±85,02 x 10^{-6} (UV-induced: 394 x 10^{-6}) 6tG-resistant clones

following UV-exposure. This protection against UV-induced mutations by Msh6 is in line with previously published work (11, 24). Loss of any of the MMR-associated proteins Mlh3, Pms1, Exo1 or Fan1 in the *Xpa* background did not result in increased spontaneous mutagenesis whereas UV-induced mutagenesis in these lines was similar to that of the *Xpa* control (Fig. 3A, 3B). Interestingly, an increase in spontaneous and UV-induced 6tG-resistant clones was observed in *XpaMlh1* cell lines (Mock: 53.91±0.47 and UV: 279.33±36.29) and *XpaPms2* (Mock: 78.81±23.23 and UV: 411.40±40.72). The increase of mutagenesis resulting from UV exposure was also significantly higher than the *Xpa* control, suggesting that not only *Msh6*, but also *Mlh1* and *Pms2* control UV-induced mutagenesis (Fig. 3B, S4B, S4D).

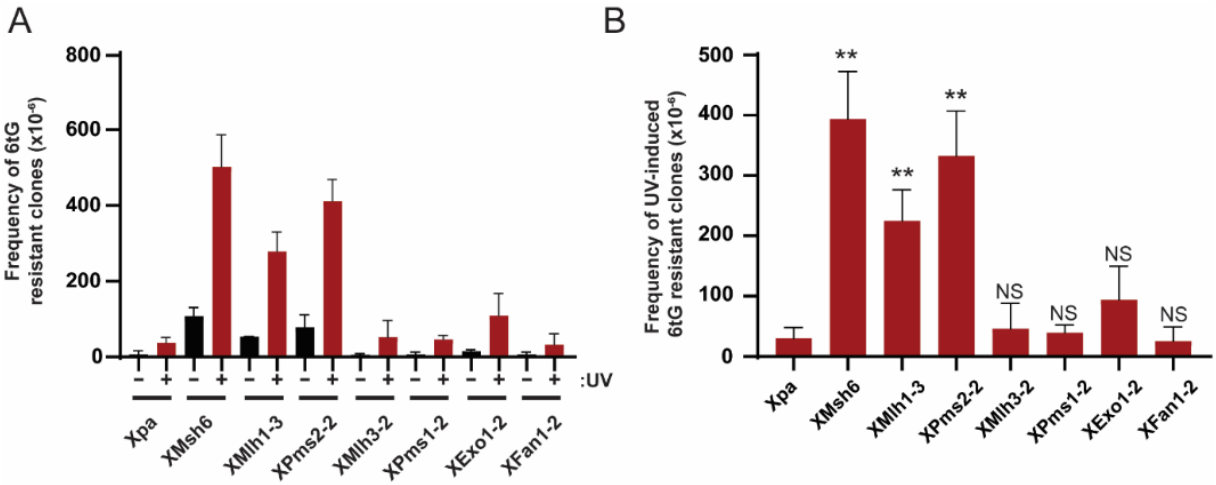

Figure 3: UV-induced mutagenesis
A: Frequency of 6tG resistant cells as a measure for mutagenesis at the Hprt gene following exposure to mock or 0,75J/M2 UVC. N=3. Error bars, SEM. B: Frequency of UV-induced 6tG resistant clones as a measure for mutagenesis at the Hprt gene. Error bars, SEM. **, P ≤ 0,01, ns, not statistically significant; unpaired T-test comparing groups to Xpa cells.

Mlh1 deficient cells display a similar spectrum of UV-induced mutations as Msh6 deficient cells

So far, our data reveal the uncoupling of ssDNA formation and checkpoint responses from the protection against UV-induced mutagenesis, suggesting mechanistic differences in the control of UV-induced mutagenesis between MutSα and MutLα. To test whether this affects the spectrum of mutations induced by UV, we studied the spontaneous and UV-induced mutational fingerprints of *Xpa*, *XpaMsh6* and *XpaMlh1* cell lines. Per genetic background and exposure status, approximately 400 6tG-resistant clones were pooled to investigate what kind of mutations inactivated *Hprt*. Using a recently published sequencing analysis pipeline (20) we identified 81 unique mutations in the UV-exposed *Xpa* cells, 32 mutations in the mock treated *XpaMsh6* cells and 31 mutations in UV-exposed *XpaMsh6* cells. Moreover, we found 70 unique mutations in mock treated and 60 unique mutations in UV-exposed *XpaMlh1*-deficient cells (Table S1-5). The spectrum of spontaneous *Hprt* mutations in an *Xpa*-deficient

background could not be determined, due to the very low number of mutants that could be selected by 6tG. These data show that double nucleotide substitutions (DNS) and multi nucleotide substitutions (MNS) were mainly found in UV-exposed cell populations whilst small insertions and deletions were associated with loss of either *XpaMsh6* or *XpaMlh1* (Fig. 4A, Table 1; Table S1-5). In all conditions tested the majority of the mutations consisted of single nucleotide substitutions (SNS). To further investigate the fingerprint of SNS in these cell lines we calculated the contribution of each type of SNS to the mutant frequency (Fig. 4B, Table 1; Table S1-5). Both mock treated *XpaMsh6* and *XpaMlh1* cells displayed a signature dominated by A.T > G.C mutations and in the case of *XpaMlh1* cells also by G.C > A.T mutations). The mutation spectra of UV-exposed *XpaMsh6* and *XpaMlh1* cells mainly consisted of G.C > A.T transitions, G.C > T.A transversions and transversions at A.T base pairs. *Xpa* cells exposed to UV displayed a spectrum consisting of G.C > A.T mutations and to a lesser extent A.T > T.A transversions and G.C > T.A transversions. To determine the spectra of UV-induced mutations we subtracted the frequency of each kind of spontaneous mutation from those observed in the UV-exposed cells (Fig. 4C; Table 1; Table S1-5). Based on this analysis we concluded that both Msh6 and Mlh1 strongly protect against UV-induced G.C > A.T transitions, G.C > T.A transversions and A.T > T.A transversions. No difference in mutational strand bias was found between *Msh6* and *Mlh1*-deficient cells. For both genotypes most of the mutations were found in the transcribed strand at dipyrimidines, which are sites where photolesions are formed following UV exposure (Fig. 4D, Table S1, 3, 5). Together, these data suggest that both Msh6 and Mlh1 protect against similar mis-incorporations that are possibly provoked by photolesions in a strand-specific fashion.

In conclusion, these data show that the activation of UV-induced DNA damage signaling and the formation of UV-induced ssDNA occurs independently of MutLα. However, the formation of UV-induced ssDNA and checkpoint activation in *Mlh1*-deficient cells does rely on *Msh6*. Moreover, MutSα and MutLα are both required for controlling UV-induced mutagenicity. Mutational fingerprints of *Msh6* and *Mlh1*-deficient cells were similar, suggesting that these proteins suppress UV-induced mutagenicity via a similar mechanism, despite the difference in the formation of ssDNA gaps.

Table 1: Distribution of base pair alterations in Xpa, XMsh6 and XMlh1 deficient backgrounds
6tG resistant clones were sequenced and mutations were distributed according to base pair substitution type and condition. The absolute number of mutations, relative proportions and mutations adjusted for the mutant frequency are shown for each base pair alteration type. The number of UVC-induced mutations is calculated by subtracting the mutations found in the mock condition from the mutations found in the UV condition.

Xpa		**Mock**			**UV**			**UV Induced**	
		Absolute	Relative (%)	6tG resistant clones ($x10^{-6}$)	Absolute	Relative	6tG resistant clones ($x10^{-6}$)	Relative (%)	6tG resistant clones ($x10^{-6}$)
Transistion	G.C > A.T	0	0	0	22	46,8	26,7	46,8	26,7
	A.T > G.C	0	0	0	2	4,3	2,4	4,3	2,4
Transversion	G.C > T.A	0	0	0	9	19,1	10,9	19,1	10,9
	G.C > C.G	0	0	0	0	0,0	0,0	0,0	0,0
	A.T > T.A	0	0	0	11	23,4	13,3	23,4	13,3
	A.T > C.G	0	0	0	3	6,4	3,6	6,4	3,6
Total		0	0	0	47	100,0	57,0	100,0	57,0

XMsh6		**Mock**			**UV**			**UV Induced**	
		Absolute	Relative (%)	6tG resistant clones ($x10^{-6}$)	Absolute	Relative	6tG resistant clones ($x10^{-6}$)	Relative (%)	6tG resistant clones ($x10^{-6}$)
Transistion	G.C > A.T	4	15,4	9,4	8	38,1	231,2	40,6	221,9
	A.T > G.C	19	73,1	44,6	1	4,8	28,9	-2,9	-15,7
Transversion	G.C > T.A	1	3,8	2,3	4	19,0	115,6	20,7	113,3
	G.C > C.G	0	0,0	0,0	1	4,8	28,9	5,3	28,9
	A.T > T.A	2	7,7	4,7	4	19,0	115,6	20,3	110,9
	A.T > C.G	0	0,0	0,0	3	14,3	86,7	15,9	86,7
Total		26	100,0	61,0	21	100,0	607,0	100,0	546,0

XMlh1		**Mock**			**UV**			**UV Induced**	
		Absolute	Relative (%)	6tG resistant clones ($x10^{-6}$)	Absolute	Relative	6tG resistant clones ($x10^{-6}$)	Relative (%)	6tG resistant clones ($x10^{-6}$)
Transistion	G.C > A.T	20	37,7	38,1	17	53,1	292,7	56,6	254,6
	A.T > G.C	20	37,7	38,1	4	12,5	68,9	6,8	30,8
Transversion	G.C > T.A	4	7,5	7,6	4	12,5	68,9	13,6	61,3
	G.C > C.G	0	0,0	0,0	0	0,0	0,0	0,0	0,0
	A.T > T.A	5	9,4	9,5	5	15,6	86,1	17,0	76,6
	A.T > C.G	4	7,5	7,6	2	6,3	34,4	6,0	26,8
Total		53	100,0	101,0	32	100,0	551,0	100,0	450,0

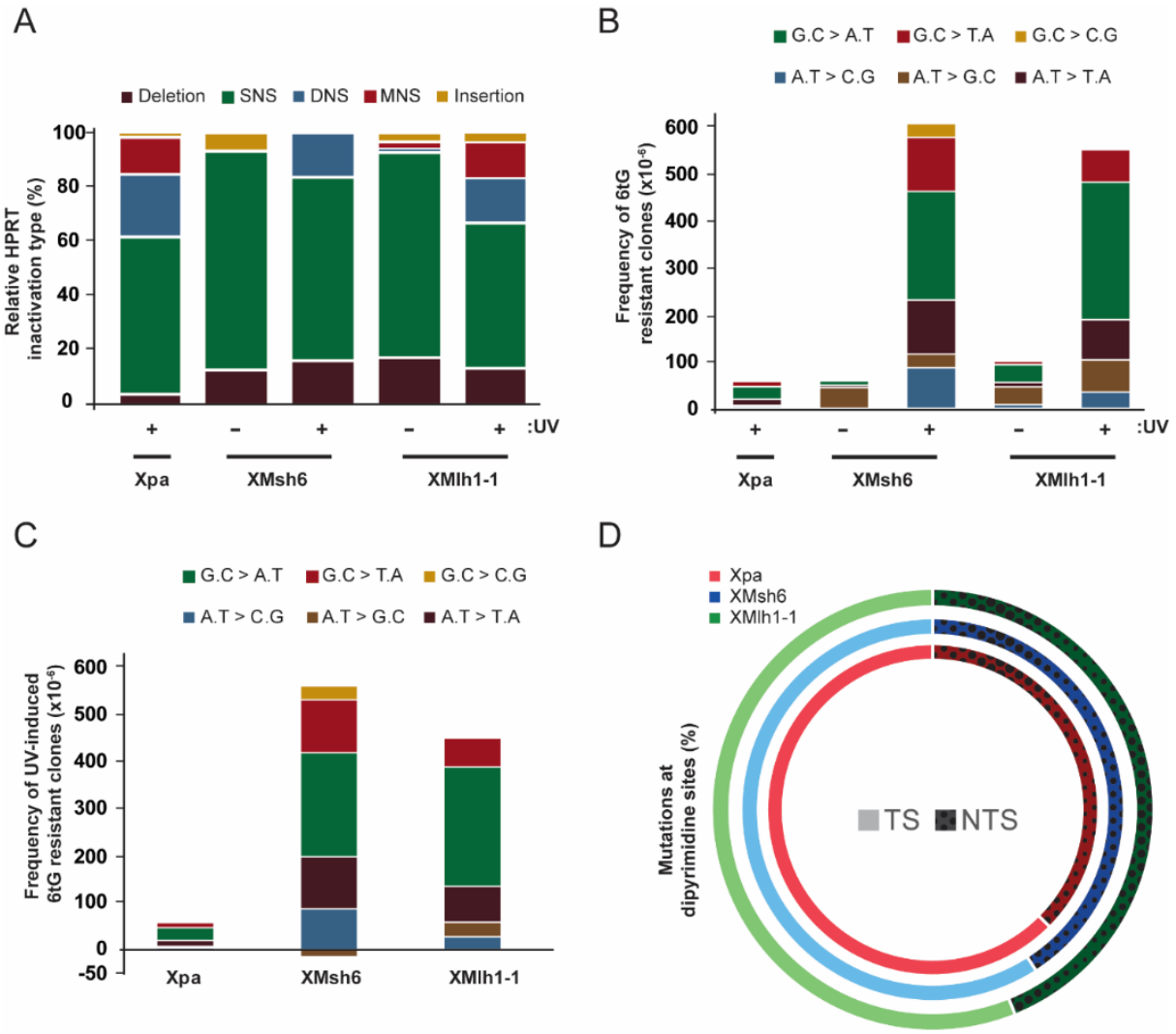

Figure 4: UVC-induced mutational fingerprints in the Hprt coding region of 6-thioguanine resistant cells
A: Percentage of mutational events in Hprt relative to the total number of unique mutants per condition. SNS, single nucleotide substitution; DNS, double nucleotide substitution; MNS, multi nucleotide substitution. B: Contribution of different base pair substitutions to the frequency of 6tG-resistant clones. C: Contribution of different base pair substitutions to the frequency of UV-induced 6tG-resistant clones. D: Mutational strand bias at Hprt in Xpa (red), XpaMsh6 (blue) and XpaMlh1 (green) deficient cells. Light colors indicate transcriptional strand (TS), dark dotted colors indicate the non-transcribed strand (NTS).

Discussion

Previous studies have shown that MutSα suppresses UV-induced mutagenesis with concomitant generation of ssDNA tracts that activate DNA damage signaling. This led to a model in which MutSα controls UV-induced mutagenesis by removing TLS-dependent misincorporations opposite UV damages, resulting in the formation of ssDNA tracts that activate DNA damage signaling (11). In the present work we have studied the roles of other MMR-related proteins, including Mlh1 and Pms2, Mlh1-interacting proteins Mlh3 and Pms1 and exonucleases Exo1 and Fan1 cells in responses to UV light. We found that in mES cells Mlh3 and Pms1 as well as MMR-related exonucleases Exo1 and Fan1 play only limited roles in UV-induced DNA damage responses, including formation of ssDNA, activation of DNA damage signaling and mutagenesis. In addition, also Mlh1 and Pms2 seem not to be important in activating UV-induced DNA damage signaling. However, MutLα does appears to play a major role in suppressing UV-induced mutagenesis. Thus, we here provide evidence that, in contrast to MutSα, MutLα seems to suppress UV-induced mutagenesis, largely independent of generation ssDNA tracts and concomitant activation of damage signaling.

In MMR-proficient cells different mechanisms may contribute to the formation of UV-induced ssDNA tracts following stalling of replicative DNA polymerases at photolesions. These mechanisms include (i) uncoupling of leading and lagging strand DNA synthesis, (ii) repriming of DNA replication downstream of the replication-blocking DNA lesion resulting in the generation of ssDNA-dsDNA junctions (25), (iii) replication fork reversal and (iv) processing of DSBs when stalled replication forks collapse (26). In the present study we noted that the appearance of chromatin-bound RPA, a read-out for ssDNA formation, strongly correlates with phosphorylation of Chk1 and Kap1 (Figs. 1, 2B, C; Fig. S2, S3B). These data implicate that the endonuclease activity of MutLα is not essential for the generation of ssDNA in response to UV-induced DNA damage. MutSα-dependent processing of stalled or collapsed replication forks might well contribute to the formation of ssDNA in Mlh1-deficient cells exposed to UV, as reported in a recent study showing that MutSα stimulates Mre11-mediated degradation of nascent DNA strands at stalled replication forks, thereby contributing to the generation of ssDNA (27). In support, we found that the formation of chromatin-bound RPA and induction of UV damage signaling was only dependent on Msh6 and not Mlh1, presumably following binding of MutSα to “compound” lesions (*i.e.* a mismatch superimposed on a UV lesion, Fig. 2B-D). The strong correlation between formation of ssDNA and activation of damage signaling makes it less likely that MMR proteins may activate an Atr/Atm-mediated UV damage response by direct interaction with Atr (Msh2) or Atm (Mlh1) as proposed for the response to methylation- or cisplatin DNA damage (21, 28). Furthermore, complete activation of the apical DNA damage signaling protein kinases Atr and Atm, that subsequently phosphorylate Chk1 and Kap1 at multiple sites (17), requires the formation of ssDNA coated with RPA (29).

Possibly, Exo-1 dependent hyper-resection that results from runaway Exo-1 activity in the absence of Mlh1, as described previously for ionizing radiation-induced responses

(23), might also contribute to the activation of UV damage signaling in Mlh1-deficient cells. In our hands, however, knock-out of Exo1 in Mlh1-deficient cells hardly altered UV damage signaling, although in MMR-proficient cells we did observe a minor role for Exo-1 in activating an UV-induced damage response, especially at early timepoints (Fig. 1, 2E). This minor role for Exo-1 may point to a functional redundancy with other exonucleases. Of note, although Exo-1 was shown to be indispensable for MMR *in vitro* (1), it seems to be non-essential for MMR in yeast and mice, in support of our data (30).

Alternatively, the presence of 5' nicks during lagging strand synthesis may provide an important clue to how cells generate UV-induced ssDNA tracts and concomitant UV damage signaling in the absence of MutLα. During canonical MMR, it is thought that MutLα is not only important in 3' nick-directed MMR but also in the generation of incisions 5' to mismatches in the newly synthesized strand (1). However, this scenario applies primarily for misincorporations during leading strand synthesis and matured Okazaki fragments, as non-ligated Okazaki fragments in the lagging strand contain naturally occurring free 5' ends. Moreover, MutLα is dispensable for 5' nick directed mismatch repair *in vitro* (Mol Cell 12, 1077-1086 (2003); Mol Cell 15, 31-41 (2004)). Lastly, several studies indicate that eukaryotic MMR acts preferentially on the lagging strand (5, 31), which might relate, in part, to MutLα-independent MMR during lagging strand DNA synthesis. For these reasons, MutLα-independent removal of mis-incorporations opposite UV lesions during lagging strand synthesis might well underly the generation of ssDNA tracts and concomitant activation of UV damage signaling observed in Mlh1-defective cells. However, MutLα-independent removal of 'misincorporations' opposite UV lesions would predict a difference in strand distribution of mutagenic UV lesions between MutSα-deficient cells versus MutSα-deficient cells; a prediction that is not confirmed by our analysis of UV-induced mutations at the coding region of the endogenous *Hprt* gene in Msh6- and Mlh1-deficient cells (Fig. 6D). Nevertheless, this difference in strand bias might be obscured in part by the plasticity of DNA replication under stressful conditions (32, 33) and by transcription-associated mutagenesis at UV lesions on the transcribed strand (34, 35).

Our mutation spectra analyses also revealed that both MutSα and, albeit to a slightly lower extent, MutLα strongly protect against UV-induced G.C > A.T transitions (Fig 4B-C; Table 1), the main type of mutation induced by UV (36). However, we also noted that MutSα and MutLα protect against transversion-type mutations, including AT > TA, AT > CG and GC > TA transversions. These transversions might rely on Rev1, a TLS polymerase that is required for the bypass of UV-induced (6-4)PPs (37, 38). Thus, whereas previously published data indicate that Msh6 removes misincorporations opposite (6-4)PPs (11), the present study suggests that also MutLα may act on TLS-induced misincorporations opposite (6-4)PPs. Combined with previous studies (11) and our findings that MutSα controls UV-induced mutagenesis and concomitantly promotes the generation of ssCPD in Polη-deficient cells (Fig. 5B, C), these data indicate that the mutagenicity of both CPDs and (6-4)PPs are controlled by MutSα and MutLα.

The spaciotemporal regulation of control of UV-induced mutagenesis by MutSα in the absence of MutLα remains to be determined. Possibly, binding of MutSα to a “compound” lesion in the absence of downstream processing by MutLα may ultimately lead to perturbed replication forks that activate DNA damage signaling. Studies using fluorescent-tagged MMR and replication proteins in replicating yeast have suggested the existence of replisome-coupled and replisome-independent (post-replicative) MutSα complexes, which recruit MutLα to perform canonical mismatch repair (5, 31). During UV-induced mutagenesis, it is thought that most mildly helix-distorting CPDs are likely bypassed by the relatively error-free TLS Polη at the fork, whereas the bypass of strongly helix-distorting (6-4)PPs depends largely on mutagenic TLS polymerases Rev1 and ζ (39-42). Possibly, the relatively rarely occurring ‘misincorporations’ opposite CPDs might be recognized by MutSα at the replication fork that, in the absence of MutLα, will lead to stalled replication complexes resulting in ssDNA formation and activation of DNA damage signaling. On the other hand, TLS at (6-4)PPs and other helix-distorting DNA lesions might occur by post-replicative gap filling (43, 44) and will result in ‘compound’ lesions that are recognized by a subset of MutSα molecules acting in a post-replicative fashion. This mode of action allows cells to continue DNA replication and, in the absence of MutLα, might not activate DNA damage signaling (For a model see Fig. 5). The idea that MutSα acts on post-replicative TLS is supported by the finding that Msh6 also suppresses the UV-induced mutagenesis in Rev1 deficient cells (11).

At present, it is not clear which MMR factors other than MutSα and MutLα play a role in controlling UV-induced mutagenesis. Here we showed that loss of Mlh3 or Pms1 did not affect DNA damage signaling nor mutagenesis in response to UV-damage. Previous work has shown that *in vitro* MLH3 is able to slightly rescue MMR activity in the absence of PMS2, and Mlh3-loss in mouse embryonic fibroblasts slightly reduces checkpoint activation and apoptosis induced by alkylating DNA damage (5, 31). However, the latter finding is contested by studies using human cell lines (36). Possibly, in mouse cells UV-induced signaling may be differently regulated than alkylation-induced signaling. As of yet, no significant role for Pms1 in MMR has been found.

Our findings that MutLα is required for suppressing mutagenesis of helix-distorting DNA lesions may provide a plausible explanation for the observation that loss of MutLα results in severely increased risk of developing colorectal cancer (45), a cancer type that strongly correlates with exposure to food-derived genotoxins that induce helix-distorting DNA lesions (46).

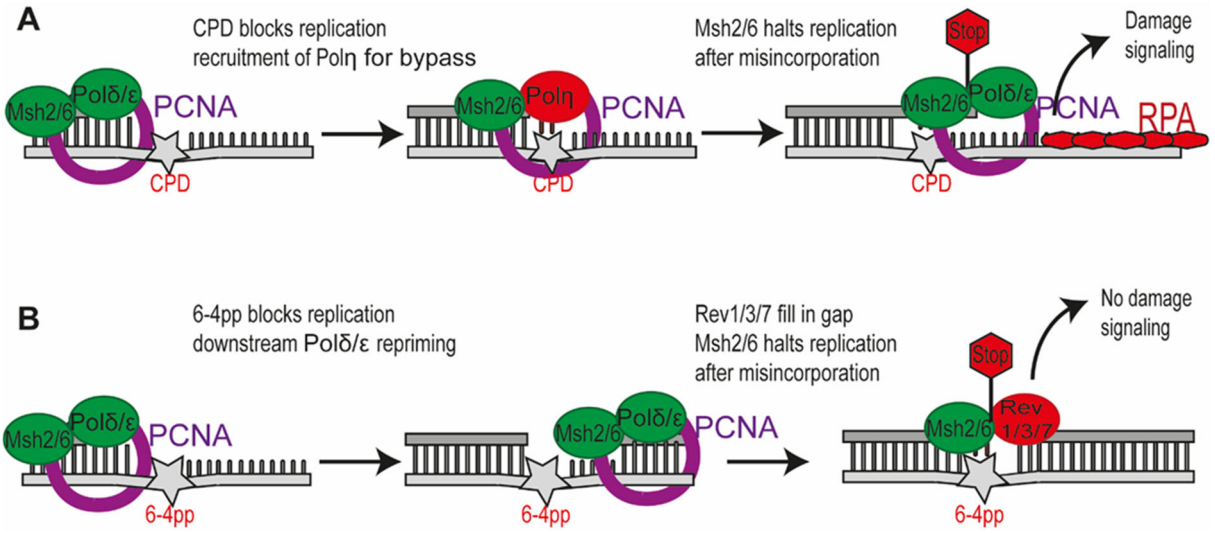

Figure 5: Different modes of bypass result in different signaling outcomes in Mlh1-deficient cells.
A: Model for the bypass of a CPD lesion in Mlh1-deficient cells. The replicative polymerases cannot continue replicating when a CPD is encountered and thus Polη is recruited to bypass the damage "on the fly". If done incorrectly, Msh2/6 halts the replication machinery causing persistent RPA-coated ssDNA tracts that activates damage signaling in the absence of Mlh1. B: Model for the bypass of a 6-4PP in Mlh1-deficient cells. When a replicative polymerase encounters a 6-4PP, repriming occurs downstream of the lesion which allows replication to continue. The resulting gap opposite the 6-4PP is filled by Rev1/3/7, quenching DNA damage signaling. In the absence of Mlh1/Pms2, 'compound' lesions are not repaired, resulting in mutation fixation in the next round of replication.

Supplemental Materials

Supplemental materials table 1: DNA sequences of PCR primers

Primer:	Sequence:
1	CGTGTGCTCTTCCGATCTTTTGCAGATTCAACTTGCGCT
2	GATGTGTATAAGAGACAGCAGTCCCAGCGTCGTGATTAG
3	CGTGTGCTCTTCCGATCTATCCAGCAGGTCAGCAAAGAA
4	GATGTGTATAAGAGACAGGCCATCACATTGTGGCCCTC
5	CGTGTGCTCTTCCGATCTAGTTTGCATTGTTTTACCAGTGTC
6	GATGTGTATAAGAGACAGTGACACTGGTAAAACAATGCAA
7	AATGATACGGCGACCACCGAGATCTACACCTCTCTATTCGTCGGCAGCGTCAGA TGTGTATAAGAGACA*G
8	CAAGCAGAAGACGGCATACGAGATagttacgtGTGACTGGAGTTCAGACGTGTGCTC TTCCGATC*T
9	AATGATACGGCGACCACCGAGATCTACACTATCCTCTTCGTCGGCAGCGTCAGA TGTGTATAAGAGACA*G
10	CAAGCAGAAGACGGCATACGAGATatacgacgGTGACTGGAGTTCAGACGTGTGCT CTTCCGATC*T
11	AATGATACGGCGACCACCGAGATCTACACAGAGTAGATCGTCGGCAGCGTCAGA TGTGTATAAGAGACA*G
12	CAAGCAGAAGACGGCATACGAGATccaactcaGTGACTGGAGTTCAGACGTGTGCT CTTCCGATC*T
13	AATGATACGGCGACCACCGAGATCTACACACTGCATATCGTCGGCAGCGTCAGA TGTGTATAAGAGACA*G
14	CAAGCAGAAGACGGCATACGAGATcgtacttcGTGACTGGAGTTCAGACGTGTGCTC TTCCGATC*T
15	AATGATACGGCGACCACCGAGATCTACACCTAAGCCTTCGTCGGCAGCGTCAGA TGTGTATAAGAGACA*G
16	CAAGCAGAAGACGGCATACGAGATgagtcatgGTGACTGGAGTTCAGACGTGTGCT CTTCCGATC*T
17	AATGATACGGCGACCACCGAGATCTACACGCGTAAGATCGTCGGCAGCGTCAGA TGTGTATAAGAGACA*G
18	CAAGCAGAAGACGGCATACGAGATgccggaacGTGACTGGAGTTCAGACGTGTGCT CTTCCGATC*T

Supplemental materials table 2: guideRNA sequences used for CRISPR

CRISPR table	*gRNA 1*	*gRNA 2*	*Target*	*Protein/mRNA*	*6tG selected*
Mlh3 lines	*TGCCCATGAACGCATTCGTT*	*-*	*Exon 6*	*No mRNA*	*No*
Pms1 lines	*AAAAAGGGCCACCAGTTCGT*	*-*	*Exon 10*	*No mRNA*	*No*
Exo1 line 1	*TATCAACATCACGCACGCC*	*-*	*Exon 5 or 6*	*Truncated mRNA*	*No*
Exo1 line 2	*TTGGCCTACCTTAACAAGGC*	*-*	*Exon 5 or 6*	*Truncated mRNA*	*No*
Fan1 lines	*CGAAGACGCGGGGATCGGCT*	*AGGGACATCTGGCCATCTAC*	*Entire gene*	*No mRNA*	*No*
Msh6 lines	*GGAGCCTCCGCTTCCCGCGG*	*CCTTTGATGGAACGTTCAT*	*Exon 1-2*	*No protein*	*Yes*
Mlh1 lines	*CTCCTCCGGAGTGAGCACGG*	*ATGCCAGATTGGACCAACTA*	*Entire gene*	*No protein*	*Yes*
Pms2 lines	*CGGCGCGCTAGACTGGACGAGGG*	*GTGAAGTCCAGGCGGCAGTTAGG*	*Exons 5-7*	*No protein*	*Yes*

Supplemental Figures

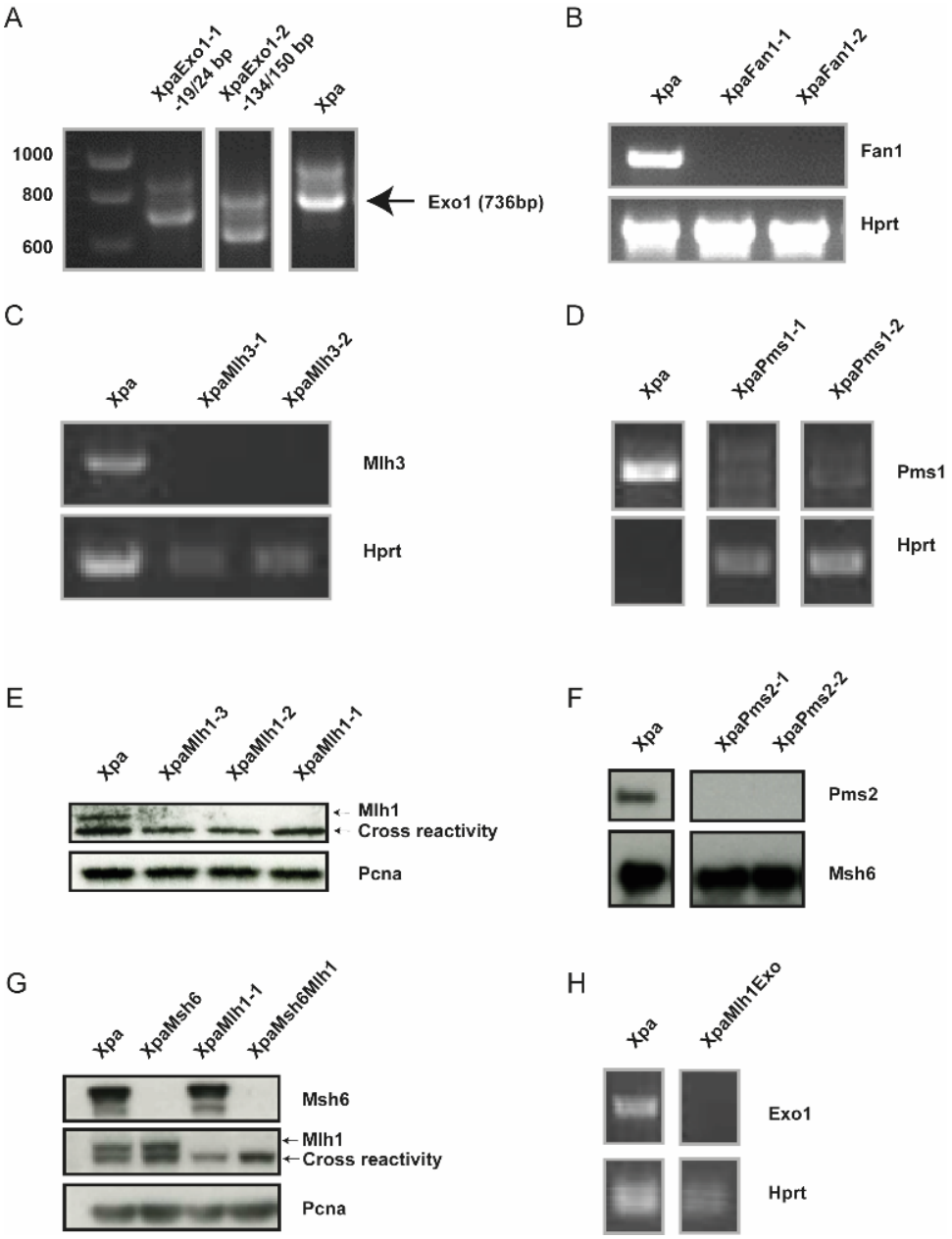

Supplemental Figure 1: Cell line validation by mRNA and protein analysis
A: Knock-out of Exo1 was validated by RT-PCR. Truncated levels of mRNA were detected, sequencing analysis showed a deletion of 19/24nt for cell line 1 and 134/150bp for cell line 2, in line with the displayed fragment sizes. B: RT-PCR analysis of Fan1 cell lines show complete loss of Fan1 mRNA. Hprt was used as a control for the presence of intact RNA. C: RT-PCR analysis of Mlh3 cell lines show complete loss of Mlh3 mRNA. D: RT-PCR analysis of Pms1 cell lines show complete loss of Pms1 mRNA. E: Western blot analysis of Mlh1 knock-out cell lines shows complete depletion of Mlh1 protein. F: Western blot analysis of Pms2 knock-out cell lines show a complete depletion of Pms2 protein. Msh6 used as loading control. G: Western blot analysis of the Msh6Mlh1 knock-out cell line shows a complete depletion of both Msh6 and Mlh1. PCNA is used as a loading control. H: mRNA analysis of the Mlh1Exo1 line showed complete lack of Exo1 mRNA. Hprt is used as a control for the presence of intact mRNA.

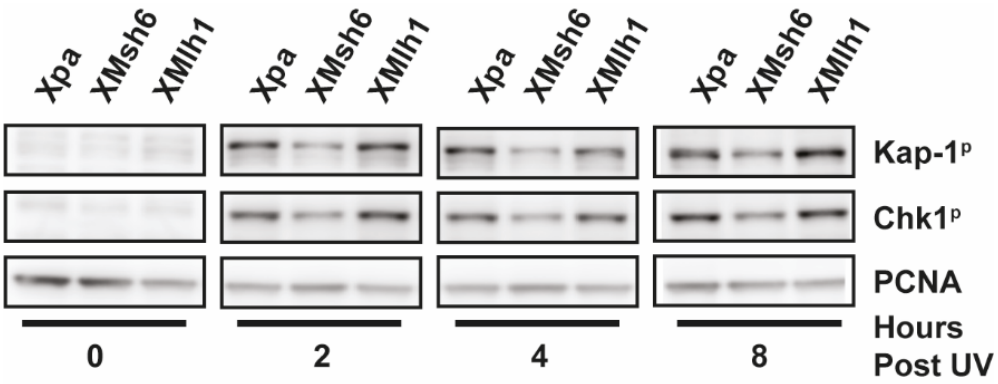

Supplemental Figure 1: UVC induced DNA damage signalling of independent cell lines
Western blots showing formation of Chk1^{p} and Kap-1^{p} in Xpa, XMsh6 and XMlh1 deficient cells, 0, 2, 4 and 8 hours post UVC exposure (0,75J/M^2). The XMlh1 cell line used is independent from the line used in Fig. 1. PCNA was used as a loading control. Representative images of 3 independent experiments. X=Xpa deficiency.

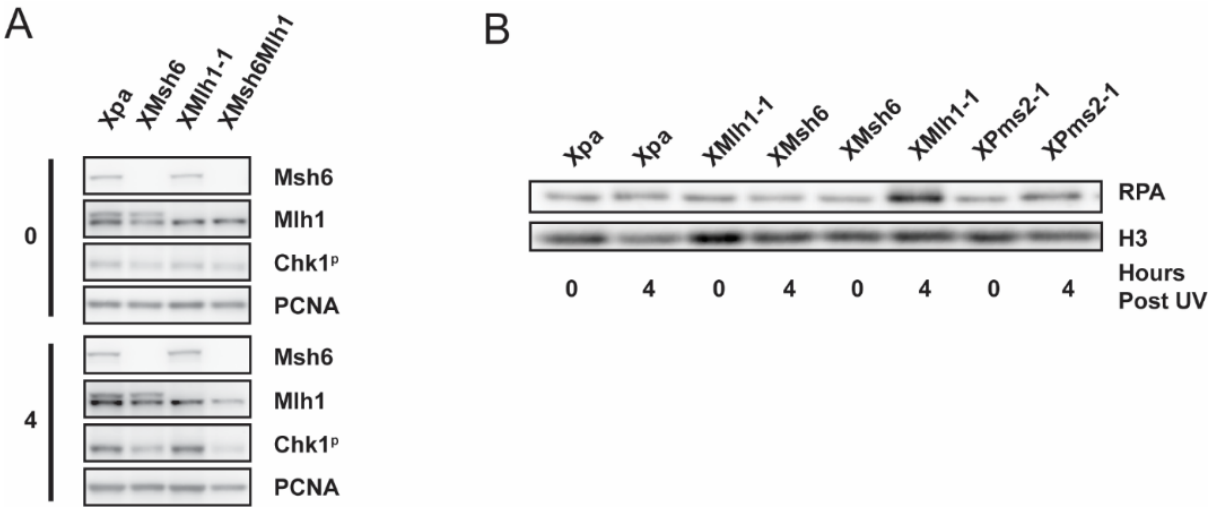

Supplemental Figure 2: UVC induced DNA damage signalling in nocodazole treated cells and chromatin-bound Rpa formation in independent MMR deficient clones.
A: Western blots showing formation of Chk1^{p} in Xpa, XMsh6 and XMlh1 and XMsh6Mlh1 deficient cells, 0 and 4 hours post UVC exposure (0,75J/M^2). Nocodazole was used in all samples to prevent mitosis and ensure measured responses are in the first cell cycle. PCNA was used as a loading control. Representative images of 3 independent experiments. X=Xpa deficiency. B: Chromatin-bound fraction of Rpa indicative of ssDNA formation at 0 and 4 hours post UVC exposure (2J/M^2). Histone H3 (H3) was used as a loading control. Representative image of three independent experiments.

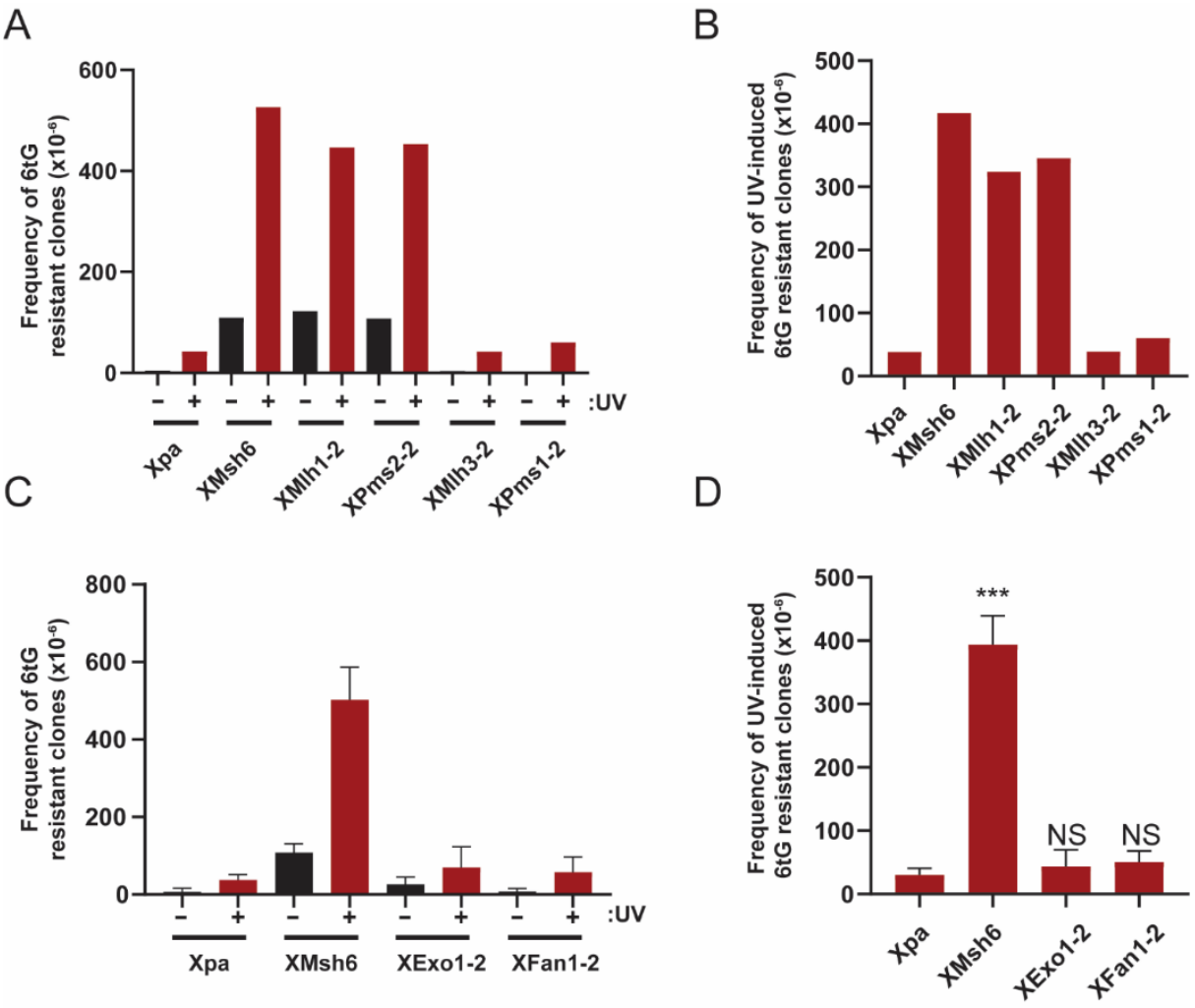

Supplemental Figure 3: UVC-induced mutagenesis in independent cell lines deficient for MMR, MMR homologs and exonucleases
*A: Frequency of 6tG resistant cells as a measure for mutagenesis at the Hprt gene in MMR and MMR homolog deficient lines following exposure to mock or 0,75J/M^2 UVC. N=1. B: Frequency of UV-induced 6tG resistant clones as a measure for mutagenesis at the Hprt gene in MMR and MMR homolog deficient lines. C: Frequency of 6tG resistant cells as a measure for mutagenesis at the Hprt gene following exposure to mock or 0,75J/M^2 UVC in exonuclease deficient cell lines. XMsh6 serves as technical control. N=3. Error bars, SEM. D: Frequency of UVC-induced 6tG resistant clones as a measure for mutagenesis at the Hprt gene in exonuclease deficient cell lines. Error bars, SEM. ***, P ≤ 0,001, ns, not statistically significant; unpaired T-test comparing groups to Xpa.*

Table S1:
List of mutants in the Hprt gene obtained after NGS of UVC-treated Xpa deficient cells and selected with 6tG for Hprt inactivation. Flanking sequence: sequence surrounding the mutated bases, parentheses surround the mutated base, non-transcribed strand sequence is shown. Strand: strand with the dipyrimidine sequence containing the mutation. NTS, non-transcribed strand. TS, transcribed strand. Dipyrimidine: mutated dipyrimidine sequence; mutated base(s) are underscored. Ins: inserted nucleotide(s), del: deleted nucleotide(s).

	Position	Exon	Base change	Flanking Sequence	Amino acid change	Strand	Dipyri-midine
SNS	40	2	G > T	GAT(G)AAC	E > *	TS	CT
	51	2	T > A	TTA(T)GAC	Y > *		
	52	2	G > T	TAT(G)ACC	D > Y	TS	CT
	69	2	T > A	TTG(T)ATA	C > *		
	74	2	C > T	TAC(C)TAA	P > L	NTS	CCT
	82	2	T > A	CAT(T)ATG	Y > N	NTS	TT
	84	2	T > G	TTA(T)GCC	Y > *		
	95	2	T > C	ATT(T)GGA	L > S	NTS	TT
	109	2	A > T	TTT(A)TTC	I > F		
	110	2	T > A	TTA(T)TCC	I > N	NTS	TT
	113	2	C > T	TTC(C)TCA	P > L	NTS	CCT
	118	2	G > A	CAT(G)GAC	G > R	TS	CC
	119	2	G > A	ATG(G)ACT	G > E	TS	CCT
	125	2	T > A	TGA(T)TAT	I > N	NTS	TT
	125	2	T > G	TGA(T)TAT	I > S	NTS	TT
	134	2	G > A	ACA(G)GAC	R > K	TS	TCC
	145	3	C > T	AGA(C)TTG	L > F	NTS	CT
	149	3	C > T	TTG(C)TCG	A > V	NTS	CT
	151	3	C > T	GCT(C)GAG	R > *	NTS	TC
	170	3	T > A	AGA(T)GGG	M > K		
	202	3	C > T	GTG(C)TCA	L > F	NTS	CT
	208	3	G > A	AAG(G)GGG	G > R	TS	CCC
SNS	209	3	G > A	AGG(G)GGG	G > E	TS	CCC
	239	3	A > T	TGG(A)TTA	D > V	TS	CT
	245	3	T > A	ACA(T)TAA	I > N	NTS	TT
	464	6	C > T	GCC(C)CAA	P > L	NTS	CCC
	482	6	C > A	TTG(C)AAG	A > E		
	527	7	C > A	GGC(C)AGA	P > Q	NTS	CC
	538	8	G > A	GTT(G)GAT	G > R	TS	CC
	539	8	G > A	TTG(G)ATT	G > E	TS	CCT
	544	8	G > A	TTT(G)AAA	E > K	TS	CT
	544	8	G > T	TTT(G)AAA	E > *	TS	CT
	547	8	A > T	GAA(A)TTC	I > F	TS	TT
	548	8	T > G	AAA(T)TCC	I > S	NTS	TT
	550	8	C > T	ATT(C)CAG	P > S	NTS	TCC
	551	8	C > A	TTC(C)AGA	P > Q	NTS	CC
	565	8	G > T	GTT(G)TTG	V > F		
	568	8	G > A	GTT(G)GAT	G > R	TS	CT
DNS	46	2	GG > TA	CCA(GG)TTA	G > Y	TS	CC

118	2	GG > AA	CAT(GG)ACT	G > K	TS	CC
169	3	AT > CA	GAG(AT)GGG	M > Q	TS	CTA
171	3	GG > AA	GAT(GG)GAG	M + G > G + R	TS	CCC
207	3	GG > AA	CAA(GG)GGG	K + G > K + R	TS	CCC
207	3	GG > AC	CAA(GG)GGG	K + G > K + R	TS	CCC
208	3	GG > AA	AAG(GG)GGG	G > K	TS	CCCC
209	3	GG > AA	AGG(GG)GGC	G > E	TS	CCCC
211	3	GG > AA	GGG(GG)CTA	G > N	TS	CCC
463	6	CC > TT	AGC(CC)CAA	P > F	NTS	CCCC
464	6	CC > TA	GCC(CC)AAA	P > L	NTS	CCC
498	7	AA > TT	GAA(AA)GGA	K + R > N + W	TS	TTTC
527	7	CA > AT	GGC(CA)GAC	P > H		CCAG
538	8	GG > AA	GTT(GG)ATT	G > K	TS	CCT
539	8	GA > TG	TTG(GA)TTT	G > V	TS	CCT
550	8	CC > TT	ATT(CC)AGA	P > L	NTS	TCC
568	8	GG > AA	GTT(GG)ATA	G > K	TS	CCT
599	8	GG > AA	TCA(GG)GAT	R > K	TS	TCCC
600	8	GG > AA	CAG(GG)ATT	R + D > R + N	TS	CCCT

	Position	Exon	Base change
MNS	44	2	CAG > AA
	113	2	CTC > TTT
	123	2	GAT > AAA
	130	2	GAC > AAA
	202	3	CTC > TTT
	229	3	GAC > AAA
	290	3	TAG > AAT
	495	7	GAAA > AAAT
	506	7	CTC > TTT
	569	8	GAT > AAA
	574	8	GCCCT > TCCCC
Insertion			
	610	9	ins AG
Deletion	486	7	del 47bp
	533	8	del 77bp
	533	8	del 21bp

Table S2:
List of mutants in the Hprt gene obtained after NGS of mock-treated XMsh6 deficient cells and selected with 6tG for Hprt inactivation. Flanking sequence: sequence surrounding the mutated bases, parentheses surround the mutated base, non-transcribed strand sequence is shown. Dipyrimidine: mutated dipyrimidine sequence; mutated base(s) are underscored. Ins: inserted nucleotide(s), del: deleted nucleotide(s).

	Position	Exon	Base change	Flanking Sequence	Amino acid change	Dipyri-midine
SNS	122	2	T > C	GAC(T)GAT	L > P	C<u>T</u>
	131	2	A > G	TGG(A)CAG	D > G	C<u>T</u>
	140	3	A > G	CTG(A)AAG	E > G	C<u>T</u>T
	154	3	G > T	CGA(G)ATG	D > Y	T<u>C</u>T
	155	3	A > G	GAG(A)TGT	D > G	C<u>T</u>
	170	3	T > C	AGA(T)GGG	M > T	
	202	3	C > T	GTG(C)TCA	L > F	<u>C</u>T
	206	3	A > G	TCA(A)GGG	K > R	T<u>C</u>C
	220	3	T > C	AAG(T)TCT	F > L	<u>T</u>T
	233	3	T > C	ACC(T)GCT	L > P	C<u>T</u>
SNS	254	3	T > C	CAC(T)GAA	L > P	C<u>T</u>
	305	3	T > A	GAC(T)GAA	L > Q	C<u>T</u>
	446	6	T > C	CCC(T)GGT	L > P	C<u>T</u>
	491	7	T > C	TGC(T)GGT	L > P	C<u>T</u>
	495	7	G > A	GGT(G)AAA	V > V	<u>C</u>T
	526	7	C > T	AGG(C)CAG	P > S	<u>C</u>C
	530	7	A > G	CAG(A)CTT	D > G	C<u>T</u>
	533	8	T > C	ACT(T)TGT	F > S	T<u>T</u>T
	544	8	G > A	TTT(G)AAA	E > K	C<u>T</u>
	563	8	T > C	TTG(T)TGT	V > A	<u>T</u>T
	572	8	A > G	GAT(A)TGC	Y > C	
	590	8	A > T	ATG(A)GTA	E > V	C<u>T</u>C
	595	8	T > C	TAC(T)TCA	F > L	C<u>T</u>T
	598	8	A > G	TTC(A)GGG	R > G	<u>T</u>C
	611	9	A > G	ATC(A)CGT	H > R	
	614	9	T > C	ACG(T)TTG	V > A	<u>T</u>T
Insertion	103	2	ins A			
	562	8	ins T			
Deletion	323	4 / 5	del 66bp			
	345	4	del A			
	486	7	del 47bp			
	533	8	del 77bp			

Table S3:
List of mutants in the Hprt gene obtained after NGS of UVC-treated XMsh6 deficient cells and selected with 6tG for Hprt inactivation. Flanking sequence: sequence surrounding the mutated bases, parentheses surround the mutated base, non-transcribed strand sequence is shown. Strand: strand with the dipyrimidine sequence containing the mutation. NTS, non-transcribed strand. TS, transcribed strand. Dipyrimidine: mutated dipyrimidine sequence; mutated base(s) are underscored. Ins: inserted nucleotide(s), del: deleted nucleotide(s).

	Position	Exon	Base change	Flanking Sequence	Amino acid change	Strand	Dipyrimi-dine
SNS	53	2	A > C	ATG(A)CCT	D > A	TS	C<u>T</u>
	71	2	T > G	GTA(T)ACC	I > R		
	71	2	T > A	GTA(T)ACC	I > K		
	122	2	T > C	GAC(T)GAT	L > P	NTS	C<u>T</u>
	139	3	G > A	ACT(G)AAA	E > K	TS	<u>C</u>T
	143	3	G > T	AAA(G)ACT	R > I	TS	T<u>C</u>T
	226	3	G > C	TTT(G)CTG	A > P		
	299	3	T > G	TTA(T)CAG	I > S	NTS	<u>T</u>C
	464	6	C > A	GCC(C)CAA	P > H	NTS	C<u>C</u>C
	472	6	G > T	ATG(G)TTA	V > F	TS	<u>CC</u>
	539	8	G > A	TTG(G)ATT	G > E	TS	C<u>C</u>T
	541	8	T > A	GGA(T)TTG	F > I	NTS	<u>TT</u>
	544	8	G > A	TTT(G)AAA	E > K	TS	<u>C</u>T
	550	8	C > T	ATT(C)CAG	P > S	NTS	<u>TCC</u>
	551	8	C > T	TTC(C)AGA	P > L	NTS	<u>CC</u>
	573	8	T > A	ATA(T)GCC	Y > *		_
	583	8	T > A	GAC(T)ATA	Y > N	NTS	<u>CT</u>
	589	8	G > A	AAT(G)AGT	E > K	TS	<u>CT</u>
	597	8	C > A	CTT(C)AGG	F > L	NTS	<u>TC</u>
	599	8	G > A	TCA(G)GGA	R > K	TS	<u>TCC</u>
	601	8	G > A	AGG(G)ATT	D > N	TS	<u>CCT</u>
DNS	208	3	GG > AA	AAG(GG)GGG	G > K	TS	<u>CCCC</u>
	209	3	GG > AA	AGG(GG)GGC	G > E	TS	<u>CCCC</u>
	464	6	CC > TT	GCC(CC)AAA	P > L	NTS	<u>CCC</u>
	538	8	GG > AA	GTT(GG)ATT	G > K	TS	<u>CCT</u>
	600	8	GG > AA	CAG(GG)ATT	R + D > R + N	TS	<u>CCCT</u>
Deletion	319	4	del 9bp				
	323	4 / 5	del 66bp				
	486	7	del 47bp				
	533	8	del 77bp				
	533	8	del 21bp				

Table S4:
List of mutants in the Hprt gene obtained after NGS of mock-treated XMlh1 deficient cells and selected with 6tG for Hprt inactivation. Flanking sequence: sequence surrounding the mutated bases, parentheses surround the mutated base, non-transcribed strand sequence is shown. Dipyrimidine: mutated dipyrimidine sequence; mutated base(s) are underscored. Ins: inserted nucleotide(s), del: deleted nucleotide(s).

	Position	Exon	Base change	Flanking Sequence	Amino acid change	Dipyrimidine
SNS	46	2	G > A	CCA(G)GTT	G > S	T<u>C</u>C
	46	2	G > T	CCA(G)GTT	G > C	T<u>C</u>C
	47	2	G > A	CAG(G)TTA	G > D	T<u>C</u>
	103	2	G > A	AAA(G)TGT	V > M	T<u>C</u>
	104	2	T > C	AAG(T)GTT	V > A	

	113	2	C > T	TTC(C)TCA	P > L	CCT
	119	2	G > T	ATG(G)ACT	G > V	CCT
	122	2	T > G	GAC(T)GAT	L > R	CT
	131	2	A > G	TGG(A)CAG	D > G	CT
	133	2	A > G	GAC(A)GGA	R > G	TC
	148	3	G > A	CTT(G)CTC	A > T	
	149	3	C > T	TTG(C)TCG	A > V	CT
	151	3	C > T	GCT(C)GAG	R > *	TC
	155	3	A > G	GAG(A)TGT	D > G	CT
	158	3	T > G	ATG(T)CAT	V > G	TC
	169	3	A > G	GAG(A)TGG	M > V	CT
	170	3	T > C	AGA(T)GGG	M > T	
	202	3	C > T	GTG(C)TCA	L > F	CT
	205	3	A > G	CTC(A)AGG	K > E	TT
	206	3	A > G	TCA(A)GGG	K > R	TTC
	208	3	G > A	AAG(G)GGG	G > R	CCC
	209	3	G > A	AGG(G)GGG	G > E	CCC
	212	3	G > A	GGG(G)CTA	G > D	CC
	215	3	A > G	GCT(A)TAA	Y > C	
	217	3	A > G	TAT(A)AGT	K > E	TT
	233	3	T > C	ACC(T)GCT	L > P	CT
	239	3	A > T	TGG(A)TTA	D > V	CT
	254	3	T > C	CAC(T)GAA	L > P	CT
	293	3	A > T	TAG(A)TTT	D > V	CT
	296	3	T > C	ATT(T)TAT	F > S	TTT
	326	4	A > C	ATC(A)GTC	Q > P	TC
	344	4	A > T	TAA(A)AGT	K > I	TTT
	355	4	G > A	GGT(G)GAG	G > R	CC
	446	4	T > C	CCC(T)GGT	L > P	CT
	463	4	C > T	AGC(C)CCA	P > S	CCC
	479	4	T > G	AGG(T)TGC	V > G	TT
	484	4	A > G	GCA(A)GCT	S > G	TTC
	491	7	T > A	TGC(T)GGT	L > Q	CT
	499	7	A > G	AAA(A)GGA	R > G	TTC
	526	7	C > T	AGG(C)CAG	P > S	CC
	533	8	T > C	ACT(T)TGT	F > S	TTT
	538	8	G > A	GTT(G)GAT	G > R	CC
	539	8	G > A	TTG(G)ATT	G > E	CCT
	544	8	G > A	TTT(G)AAA	E > K	CT
	569	8	G > A	TTG(G)ATA	G > E	CCT
	572	8	A > G	GAT(A)TGC	Y > C	
	577	8	C > T	GCC(C)TTG	L > F	CCT
	595	8	T > A	TAC(T)TCA	F > I	CTT
	598	8	A > G	TTC(A)GGG	R > G	TC
	599	8	G > T	TCA(G)GGA	R > M	TCC
	599	8	G > A	TCA(G)GGA	R > K	TCC
	600	8	G > T	CAG(G)GAT	R > S	CCC
	605	8	T > C	ATT(T)GAA	L > S	TT
	550	8	CC > TT	ATT(CC)AGA	P > L	TCC

Table S4 continued:

	Position	Exon	Base change
MNS	541	8	TTT > ATA
	581	8	AC > TTTT
Insertion	96	2	ins T
	500	7	ins A
Deletion	101	2	del AA
	208	3	del 111bp
	319	4	del 9bp
	323	4 / 5	del 66bp
	337	4	G
	345	4	A
	486	7	del 47bp
	499	7	A
	533	8	del 77bp
	533	8	del 21bp
	547	8	del A
	586	8	del AAT

Table S5:
List of mutants in the Hprt gene obtained after NGS of UVC-treated XMlh1 deficient cells and selected with 6tG for Hprt inactivation. Flanking sequence: sequence surrounding the mutated bases, parentheses surround the mutated base, non-transcribed strand sequence is shown. Strand: strand with the dipyrimidine sequence containing the mutation. NTS, non-transcribed strand. TS, transcribed strand. Dipyrimidine: mutated dipyrimidine sequence; mutated base(s) are underscored. Ins: inserted nucleotide(s), del: deleted nucleotide(s).

	Position	Exon	Base change	Flanking Sequence	Amino acid change	Strand	Dipyrimidine
SNS	52	2	G > T	TAT(G)ACC	D > Y	TS	CT
	67	2	T > C	TTT(T)GTA	C > R	NTS	TT
	74	2	C > T	TAC(C)TAA	P > L	NTS	CCT
	118	2	G > A	CAT(G)GAC	G > R	TS	CC
	139	3	G > A	ACT(G)AAA	E > K	TS	CT
	140	3	A > T	CTG(A)AAG	E > V	TS	CTT
	145	3	C > T	AGA(C)TTG	L > F	NTS	CT
	151	3	C > T	GCT(C)GAG	R > *	NTS	TC
	163	3	A > T	ATG(A)AGG	K > *	TS	CTT
	182	3	A > T	ATC(A)CAT	H > L		
	212	3	G > A	GGG(G)CTA	G > D	TS	CC
	281	3	C > A	TTC(C)TAT	P > H	NTS	CCT
	355	4	G > A	GGT(G)GAG	G > R	TS	CC
	464	4	C > T	GCC(C)CAA	P > L	NTS	CCC
	475	4	A > G	GTT(A)AGG	K > E	TS	TT
	508	7	C > T	TCT(C)GAA	R > *	NTS	TC
	526	7	C > T	AGG(C)CAG	P > S	NTS	CC
	539	8	G > A	TTG(G)ATT	G > E	TS	CCA
	544	8	G > A	TTT(G)AAA	E > K	TS	CT
	544	8	G > T	TTT(G)AAA	E > *	TS	CT
	547	8	A > T	GAA(A)TTC	I > F	TS	TT
	548	8	T > A	AAA(T)TCC	I > N	NTS	TT
	548	8	T > G	AAA(T)TCC	I > S	NTS	TT
	550	8	C > T	ATT(C)CAG	P > S	NTS	TCC
	569	8	G > A	TTG(G)ATA	G > E	TS	CCT
	574	8	G > A	TAT(G)CCC	A > T		
	577	8	C > T	GCC(C)TTG	L > F	NTS	CCT
	589	8	G > A	AAT(G)AGT	E > K	TS	CT
	595	8	T > C	TAC(T)TCA	F > L	NTS	CCT
	596	8	T > G	ACT(T)CAG	F > C	NTS	TTC
	596	8	T > C	ACT(T)CAG	F > S	NTS	TTC
	597	8	C > A	CTT(C)AGG	F > L	NTS	TC

Table S5 continued:

	Position	Exon	Base change	Flanking Sequence	Amino acid change	Strand	Dipyrimidine
DNS	84	2	TG > AT	TTA(TG)CCG	Y + A > * + S		
	118	2	GG > AA	CAT(GG)ACT	G > K	TS	CCT
	157	3	GT > TA	GAT(GT)CAT	V > Y	NTS	CAG
	165	3	GG > AA	GAA(GG)AGA	K + E > K + K	TS	TCCT
	208	3	GG > AA	AAG(GG)GGG	G > K	TS	CCCC
	538	8	GG > AA	GTT(GG)ATT	G > K	TS	CCT
	568	8	GG > AA	GTT(GG)ATA	G > K		CCT
	573	8	TG > AT	ATA(TG)CCC	Y + A > * + S		
	600	8	GG > AA	CAG(GG)ATT	R + D > R + N	TS	CCCT
	611	9	AC > TT	ATC(AC)GTT	H > L		
MNS	97	2	G > AA				
	113	2	CTC > TT				
	130	2	GAC > AAA				
	202	3	CTC > TTT				
	205	3	A > CAG				
	207	3	GGG > TAA				
	229	3	GAC > AAA				
	544	8	GA > T				
Insertion	103	2	ins T				
	500	7	ins A				
Deletion	127	2	del A				
	208	3	del 111bp				
	319	4	del 9bp				
	323	4 / 5	del 66bp				
	337	4	del G				
	486	5 / 6 / 7	del 47bp				
	533	8	del 77bp				
	533	8	del 21bp				

References

1. Zhang Y, Yuan F, Presnell SR, Tian K, Gao Y, Tomkinson AE, et al. Reconstitution of 5′-Directed Human Mismatch Repair in a Purified System. Cell. 2005;122(5):693-705.
2. Goellner EM, Putnam CD, Kolodner RD. Exonuclease 1-dependent and independent mismatch repair. DNA Repair (Amst). 2015;32:24-32.
3. Rikitake M, Fujikane R, Obayashi Y, Oka K, Ozaki M, Hidaka M. MLH1-mediated recruitment of FAN1 to chromatin for the induction of apoptosis triggered by O(6) -methylguanine. Genes to cells : devoted to molecular & cellular mechanisms. 2020;25(3):175-86.
4. Kadyrova LY, Gujar V, Burdett V, Modrich PL, Kadyrov FA. Human MutLgamma, the MLH1-MLH3 heterodimer, is an endonuclease that promotes DNA expansion. Proc Natl Acad Sci U S A. 2020;117(7):3535-42.
5. Chen PC, Dudley S, Hagen W, Dizon D, Paxton L, Reichow D, et al. Contributions by MutL homologues Mlh3 and Pms2 to DNA mismatch repair and tumor suppression in the mouse. Cancer Res. 2005;65(19):8662-70.
6. Prolla TA, Baker SM, Harris AC, Tsao JL, Yao X, Bronner CE, et al. Tumour susceptibility and spontaneous mutation in mice deficient in Mlh1, Pms1 and Pms2 DNA mismatch repair. Nat Genet. 1998;18(3):276-9.
7. Friedberg EC. Suffering in silence: the tolerance of DNA damage. Nature Reviews Molecular Cell Biology. 2005;6(12):943-53.
8. Wang H, Lawrence CW, Li GM, Hays JB. Specific binding of human MSH2.MSH6 mismatch-repair protein heterodimers to DNA incorporating thymine- or uracil-containing UV light photoproducts opposite mismatched bases. J Biol Chem. 1999;274(24):16894-900.
9. Seifert M, Scherer SJ, Edelmann W, Bohm M, Meineke V, Lobrich M, et al. The DNA-mismatch repair enzyme hMSH2 modulates UV-B-induced cell cycle arrest and apoptosis in melanoma cells. The Journal of investigative dermatology. 2008;128(1):203-13.
10. van Oosten M, Stout GJ, Backendorf C, Rebel H, de Wind N, Darroudi F, et al. Mismatch repair protein Msh2 contributes to UVB-induced cell cycle arrest in epidermal and cultured mouse keratinocytes. DNA Repair (Amst). 2005;4(1):81-9.
11. Tsaalbi-Shtylik A, Ferras C, Pauw B, Hendriks G, Temviriyanukul P, Carlee L, et al. Excision of translesion synthesis errors orchestrates responses to helix-distorting DNA lesions. J Cell Biol. 2015;209(1):33-46.
12. Nara K, Nagashima F, Yasui A. Highly elevated ultraviolet-induced mutation frequency in isolated Chinese hamster cell lines defective in nucleotide excision repair and mismatch repair proteins. Cancer Res. 2001;61(1):50-2.
13. Borgdorff V, Pauw B, van Hees-Stuivenberg S, de Wind N. DNA mismatch repair mediates protection from mutagenesis induced by short-wave ultraviolet light. DNA Repair (Amst). 2006;5(11):1364-72.
14. Shin-Darlak CY, Skinner AM, Turker MS. A role for Pms2 in the prevention of tandem CC --> TT substitutions induced by ultraviolet radiation and oxidative stress. DNA Repair (Amst). 2005;4(1):51-7.
15. Meira LB, Cheo DL, Reis AM, Claij N, Burns DK, te Riele H, et al. Mice defective in the mismatch repair gene Msh2 show increased predisposition to UVB radiation-induced skin cancer. DNA Repair (Amst). 2002;1(11):929-34.
16. Yoshino M, Nakatsu Y, te Riele H, Hirota S, Kitamura Y, Tanaka K. Additive roles of XPA and MSH2 genes in UVB-induced skin tumorigenesis in mice. DNA Repair (Amst). 2002;1(11):935-40.
17. Smith J, Tho LM, Xu N, Gillespie DA. The ATM-Chk2 and ATR-Chk1 pathways in DNA damage signaling and cancer. Advances in cancer research. 2010;108:73-112.
18. Hooper M, Hardy K, Handyside A, Hunter S, Monk M. HPRT-deficient (Lesch-Nyhan) mouse embryos derived from germline colonization by cultured cells. Nature. 1987;326(6110):292-5.
19. Magoc T, Salzberg SL. FLASH: fast length adjustment of short reads to improve genome assemblies. Bioinformatics. 2011;27(21):2957-63.
20. van Schendel R, Schimmel J, Tijsterman M. SIQ: easy quantitative measurement of mutation profiles in sequencing data. NAR genomics and bioinformatics. 2022;4(3):lqac063.
21. Wang Y, Qin J. MSH2 and ATR form a signaling module and regulate two branches of the damage response to DNA methylation. Proc Natl Acad Sci U S A. 2003;100(26):15387-92.
22. Ciccia A, Elledge SJ. The DNA damage response: making it safe to play with knives. Mol Cell. 2010;40(2):179-204.
23. Guan J, Lu C, Jin Q, Lu H, Chen X, Tian L, et al. MLH1 Deficiency-Triggered DNA Hyperexcision by Exonuclease 1 Activates the cGAS-STING Pathway. Cancer Cell. 2021;39(1):109-21 e5.
24. Borgdorff V, van Hees-Stuivenberg S, Meijers CM, de Wind N. Spontaneous and mutagen-induced loss of DNA mismatch repair in Msh2-heterozygous mammalian cells. Mutat Res. 2005;574(1-2):50-7.
25. Elvers I, Johansson F, Groth P, Erixon K, Helleday T. UV stalled replication forks restart by re-priming in human fibroblasts. Nucleic Acids Res. 2011;39(16):7049-57.
26. Liao H, Ji F, Helleday T, Ying S. Mechanisms for stalled replication fork stabilization: new targets for synthetic lethality strategies in cancer treatments. EMBO reports. 2018;19(9).
27. Zhang J, Zhao X, Liu L, Li HD, Gu L, Castrillon DH, et al. The mismatch recognition protein MutSalpha promotes nascent strand degradation at stalled replication forks. Proc Natl Acad Sci U S A. 2022;119(40):e2201738119.
28. Wu Q, Vasquez KM. Human MLH1 protein participates in genomic damage checkpoint signaling in response to DNA interstrand crosslinks, while MSH2 functions in DNA repair. PLoS Genet. 2008;4(9):e1000189.
29. Shiotani B, Zou L. ATR signaling at a glance. J Cell Sci. 2009;122(Pt 3):301-4.

30. Li Z, Pearlman AH, Hsieh P. DNA mismatch repair and the DNA damage response. DNA Repair (Amst). 2016;38:94-101.
31. Cannavo E, Marra G, Sabates-Bellver J, Menigatti M, Lipkin SM, Fischer F, et al. Expression of the MutL homologue hMLH3 in human cells and its role in DNA mismatch repair. Cancer Res. 2005;65(23):10759-66.
32. Yekezare M, Gomez-Gonzalez B, Diffley JF. Controlling DNA replication origins in response to DNA damage - inhibit globally, activate locally. J Cell Sci. 2013;126(Pt 6):1297-306.
33. Berti M, Cortez D, Lopes M. The plasticity of DNA replication forks in response to clinically relevant genotoxic stress. Nature reviews Molecular cell biology. 2020;21(10):633-51.
34. Hendriks G, Calleja F, Besaratinia A, Vrieling H, Pfeifer GP, Mullenders LH, et al. Transcription-dependent cytosine deamination is a novel mechanism in ultraviolet light-induced mutagenesis. Current biology : CB. 2010;20(2):170-5.
35. Hendriks G, Calleja F, Vrieling H, Mullenders LH, Jansen JG, de Wind N. Gene transcription increases DNA damage-induced mutagenesis in mammalian stem cells. DNA Repair (Amst). 2008;7(8):1330-9.
36. Roesner LM, Mielke C, Fahnrich S, Merkhoffer Y, Dittmar KE, Drexler HG, et al. Stable expression of MutLgamma in human cells reveals no specific response to mismatched DNA, but distinct recruitment to damage sites. Journal of cellular biochemistry. 2013;114(10):2405-14.
37. Jansen JG, Tsaalbi-Shtylik A, Langerak P, Calleja F, Meijers CM, Jacobs H, et al. The BRCT domain of mammalian Rev1 is involved in regulating DNA translesion synthesis. Nucleic Acids Res. 2005;33(1):356-65.
38. Temviriyanukul P, van Hees-Stuivenberg S, Delbos F, Jacobs H, de Wind N, Jansen JG. Temporally distinct translesion synthesis pathways for ultraviolet light-induced photoproducts in the mammalian genome. DNA Repair (Amst). 2012;11(6):550-8.
39. Jansen JG, Fousteri MI, de Wind N. Send in the clamps: control of DNA translesion synthesis in eukaryotes. Mol Cell. 2007;28(4):522-9.
40. Shachar S, Ziv O, Avkin S, Adar S, Wittschieben J, Reissner T, et al. Two-polymerase mechanisms dictate error-free and error-prone translesion DNA synthesis in mammals. EMBO J. 2009;28(4):383-93.
41. Despras E, Daboussi F, Hyrien O, Marheineke K, Kannouche PL. ATR/Chk1 pathway is essential for resumption of DNA synthesis and cell survival in UV-irradiated XP variant cells. Human molecular genetics. 2010;19(9):1690-701.
42. Jansen JG, Tsaalbi-Shtylik A, Hendriks G, Gali H, Hendel A, Johansson F, et al. Separate domains of Rev1 mediate two modes of DNA damage bypass in mammalian cells. Mol Cell Biol. 2009;29(11):3113-23.
43. Quinet A, Martins DJ, Vessoni AT, Biard D, Sarasin A, Stary A, et al. Translesion synthesis mechanisms depend on the nature of DNA damage in UV-irradiated human cells. Nucleic Acids Res. 2016;44(12):5717-31.
44. Tirman S, Quinet A, Wood M, Meroni A, Cybulla E, Jackson J, et al. Temporally distinct post-replicative repair mechanisms fill PRIMPOL-dependent ssDNA gaps in human cells. Mol Cell. 2021;81(19):4026-40 e8.
45. Win AK, Jenkins MA, Dowty JG, Antoniou AC, Lee A, Giles GG, et al. Prevalence and Penetrance of Major Genes and Polygenes for Colorectal Cancer. Cancer Epidemiol Biomarkers Prev. 2017;26(3):404-12.
46. Chiavarini M, Bertarelli G, Minelli L, Fabiani R. Dietary Intake of Meat Cooking-Related Mutagens (HCAs) and Risk of Colorectal Adenoma and Cancer: A Systematic Review and Meta-Analysis. Nutrients. 2017;9(5):514.